ChemPubSoc Europe
DOI: 10.1002/chem.201303607
CHEMISTRY
A European Journal
Full Paper

Fluorescence

Tunable Fluorophores Based on 2-(*N*-Arylimino)pyrrolyl Chelates of Diphenylboron: Synthesis, Structure, Photophysical Characterization, and Application in OLEDs

D. Suresh,[a] Patrícia S. Lopes,[a] Bruno Ferreira,[a] Cláudia A. Figueira,[a] Clara S. B. Gomes,[a] Pedro T. Gomes,*[a] Roberto E. Di Paolo,[a] António L. Maçanita,[a] M. Teresa Duarte,[a] Ana Charas,[b] Jorge Morgado,[b, c] and Maria José Calhorda[d]

Abstract: Reactions of 2-(*N*-arylimino)pyrroles ($HNC_4H_3C(H){=}N\text{-}Ar$) with triphenylboron ($BPh_3$) in boiling toluene afford the respective highly emissive *N*,*N*′-boron chelate complexes, $[BPh_2\{\kappa^2 N,N'\text{-}NC_4H_3C(H){=}N\text{-}Ar\}]$ (Ar = C_6H_5 (**12**), 2,6-Me_2-C_6H_3 (**13**), 2,6-*i*Pr_2-C_6H_3 (**14**), 4-OMe-C_6H_4 (**15**), 3,4-Me_2-C_6H_3 (**16**), 4-F-C_6H_4 (**17**), 4-NO_2-C_6H_4 (**18**), 4-CN-C_6H_4 (**19**), 3,4,5-F_3-C_6H_2 (**20**), and C_6F_5 (**21**)) in moderate to high yields. The photophysical properties of these new boron complexes largely depend on the substituents present on the aryl rings of their *N*-arylimino moieties. The complexes bearing electron-withdrawing aniline substituents **17**–**20** show more intense (e.g., $\phi_f = 0.71$ for Ar = 4-CN-C_6H_4 (**19**) in THF), higher-energy (blue) fluorescent emission compared to those bearing electron-donating substituents, for which the emission is red-shifted at the expense of lower quantum yields ($\phi_f = 0.13$ and 0.14 for Ar = 4-OMe-C_6H_4 (**15**) and 3,4-Me_2-C_6H_3 (**16**), respectively, in THF). The presence of substituents bulkier than a hydrogen atom at the 2,6-positions of the aryl groups strongly restricts rotation of this moiety towards coplanarity with the iminopyrrolyl ligand framework, inducing a shift in the emission to the violet region ($\lambda_{max} = 410$–465 nm) and a significant decrease in quantum yield ($\phi_f = 0.005$, 0.023, and 0.20 for Ar = 2,6-Me_2-C_6H_3 (**13**), 2,6-*i*Pr_2-C_6H_3 (**14**), and C_6F_5 (**21**), respectively, in THF), even when electron-withdrawing groups are also present. Density functional theory (DFT) and time-dependent DFT (TD-DFT) calculations have indicated that the excited singlet state has a planar aryliminopyrrolyl ligand, except when prevented by steric hindrance (*ortho* substituents). Calculated absorption maxima reproduce the experimental values, but the error is higher for the emission wavelengths. Organic light-emitting diodes (OLEDs) have been fabricated with the new boron complexes, with luminances of the order of 3000 $cd\,m^{-2}$ being achieved for a green-emitting device.

Introduction

There has been considerable interest in the synthesis of bidentate chelating ligands containing an imine and a donor moiety, in order to prepare organometallic complexes that might be applied as pre-catalysts for various organic reactions.[1] Bidentate 2-iminopyrrolyl chelating ligands, containing a pyrrolyl anionic ring and a neutral imine as donor moieties, are one such type of ligands,[2] which can be considered to be structurally similar to salicylaldiminate, anilidoimine, or 2-(2-pyridyl)indolyl ligands.[3] Although the first syntheses of homoleptic metal complexes of Co^{II}, Ni^{II}, Pd^{II}, Cu^{II}, and Zn^{II} containing ligands of this kind were reported back in the 1960s,[4] there has been a recent resurgence of interest in such systems.[5] The ease of steric and electronic tuning through the introduction of aryl substituents on the imine group makes these chelates highly flexible in terms of ligand design, which renders them very interesting for various applications. For instance, bulky aryl substituents on the imine group provide steric tuning and shielding of the metal centers and hence several mono- or bis-[2-(*N*-arylimino)pyrrolyl] early and late transition-metal complexes have been reported in the literature as efficient α-olefin oligo-/polymerization catalysts.[2,6]

Besides catalytic investigation, another important focus of interest in recent years has been the synthesis of coordination and organometallic compounds with photoluminescent (PL)

---

[a] Dr. D. Suresh, P. S. Lopes, B. Ferreira, C. A. Figueira, Dr. C. S. B. Gomes, Dr. P. T. Gomes, Dr. R. E. Di Paolo, Prof. A. L. Maçanita, Dr. M. T. Duarte
Centro de Química Estrutural
Departamento de Engenharia Química
Instituto Superior Técnico, Universidade de Lisboa
Av. Rovisco Pais, 1049-001 Lisboa (Portugal)
E-mail: pedro.t.gomes@tecnico.ulisboa.pt

[b] Dr. A. Charas, Dr. J. Morgado
Instituto de Telecomunicações
Av. Rovisco Pais, 1049-001 Lisboa (Portugal)

[c] Dr. J. Morgado
Department of Bioengineering, Instituto Superior Técnico
Universidade de Lisboa
Av. Rovisco Pais, 1049-001 Lisboa (Portugal)

[d] Prof. M. J. Calhorda
Departamento de Química e Bioquímica, CQB
Faculdade de Ciências, Universidade de Lisboa
Campo Grande, Ed. C8, 1749-016 Lisboa (Portugal)

Supporting information for this article is available on the WWW under http://dx.doi.org/10.1002/chem.201303607.

properties, due to their potential applications in electroluminescent (EL) displays.[7] Luminescent chelate complexes have proved to be particularly useful in electroluminescent displays because of their relatively high stability and volatility.[8] Much effort has been devoted to the design and synthesis of new phosphorescent materials with heavy metals such as iridium(III)[9] and platinum(II).[10] Recently, the synthesis of fluorescent tricoordinate[11] and tetracoordinate[12] boron complexes has attracted a great deal of attention because of their potential applications in functional materials and in sensors.[13] Earlier reports on boron-based complexes suggested that variations in the chromophore part of the molecule would influence the HOMO–LUMO levels and thereby the color of emission.[12a,d] In addition, some of these compounds exhibited good charge-transport properties and, consequently, could be employed in the fabrication of organic light-emitting diodes (OLEDs) and sensors.[14]

Recently, we have developed new homoleptic 2-(*N*-arylformimino)pyrrolyl zinc(II) complexes of the type [Zn{κ^2*N*,*N*′-2-(*N*-arylformimino)pyrrolyl}$_2$] (**A1** and **A2**) or [Zn{κ^2*N*,*N*′-2-(*N*-arylformimino)phenanthro[9,10-*c*]pyrrolyl}$_2$] (**A3** and **A4**), the latter containing a phenanthrene fragment fused on the C3–C4 bond of the pyrrolyl ring of the ligand, and studied their photoluminescent properties.[15] The two phenanthrene-fused iminopyrrolyl zinc complexes showed mainly a ligand-based $^1(\pi-\pi^*)$ emission in the blue/green spectral region, but their fluorescence efficiencies were low ($\phi_f = 3.9$ and 8.8%, respectively). Eisenberg and co-workers reported a series of neutral phosphorescent copper(I) complexes of the types [Cu(N,N)(P,P)] and [Cu(N,O)(P,P)] containing phosphine or diphosphine ligands and coordinated bidentate N,N ancillary ligands such as 2-(*N*-phenylformimino)pyrrolyl or 2-(*N*-phenylformimino)indolyl (**B**), or the corresponding parent bidentate N,O ancillary ligands 2-formylpyrrolyl or 2-formylindolyl, respectively (**C**).[16] These complexes exhibited long-lived emissions, the excited states of which could be assigned to mixed intraligand $^3(\pi-\pi^*)$ and metal-to-ligand charge-transfer (MLCT) transitions. Their phosphorescence quantum yields were, however, very low ($\phi_p < 3\%$). Experimental and theoretical results indicated that the photophysical properties of these complexes largely depended on the N,N or N,O anionic ancillary ligands.

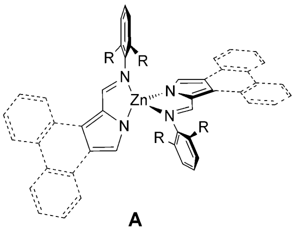

A

A1 R = H
A2 R = *i*Pr
A3 R = H
A4 R = *i*Pr } = Phen

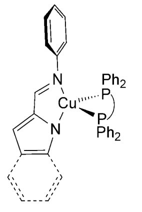

B

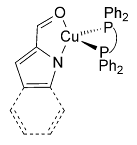

C

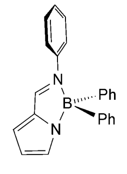

D

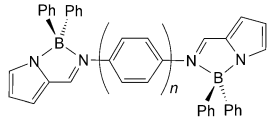

E

n=1
n=2

Very recently, in a preliminary communication, we reported the synthesis and characterization of new fluorescent four-coordinate mono- and binuclear organoboron complexes containing 2-(*N*-arylformimino)pyrrolyl bidentate ligands (**D** and **E**, respectively) and their successful application in single-layer, non-doped OLEDs.[17] In particular, the mononuclear boron complex [BPh$_2${κ^2*N*,*N*′-NC$_4$H$_3$C(H)=N-Ph}] **D** (denoted as **12** in the present work; see Scheme 2 below) exhibited blue fluorescence ($\lambda_{em}^{max} = 479$ nm) characterized by a quantum yield of 34%, this emission being assigned to a virtually pure ligand-based $^1(\pi-\pi^*)$ transition.[18]

These results prompted us to synthesize new boron complexes containing 2-(*N*-arylformimino)pyrrolyl anionic ligands and, in order to assess their emissivity and color tunability, to study in detail their photoluminescent properties under the influence of different structural parameters of the *N*-aryl ring. In the present paper, we report a series of highly emissive mononuclear 2-(*N*-arylformimino)pyrrolyl chelates of diphenylboron, [BPh$_2${κ^2*N*,*N*′-NC$_4$H$_3$C(H)=N-Ar}], and their characterization by multinuclear NMR, X-ray diffraction analysis, and cyclic voltammetry. Photophysical characterization of the newly synthesized complexes was accomplished by steady-state and time-resolved luminescence techniques in solution. Density functional theory (DFT) and time-dependent DFT (TD-DFT) calculations (ADF program) were also carried out on these new boron complexes, to assign their electronic transitions and to determine their singlet excited-state properties (geometry, lifetime, emission). Furthermore, these compounds have been utilized as emissive layers in OLED devices.

Results and Discussion

Synthesis and characterization of iminopyrrole ligand precursors

Most of the ligand precursors were synthesized and characterized according to literature methods (Scheme 1).[5d,19–24] The new ligand precursors **6** and **10** were synthesized, and their characterization data are presented in the Experimental Section. In general, the 2-(*N*-arylformimino)pyrrole ligand precur-

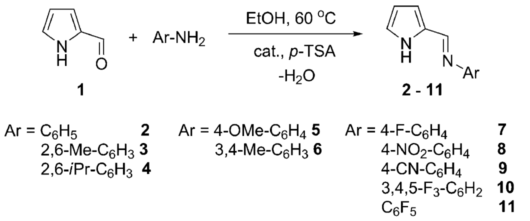

Scheme 1. Synthesis of 2-(*N*-arylformimino)pyrrole ligand precursors **2–11**. *p*-TSA = *para*-toluenesulfonic acid.

sors ($HNC_4H_3C(H){=}N$-Ar), with Ar = C_6H_5 (**2**), 2,6-Me_2-C_6H_3 (**3**), 2,6-*i*Pr_2-C_6H_3 (**4**), 4-OMe-C_6H_4 (**5**), 3,4-Me_2-C_6H_3 (**6**), 4-F-C_6H_4 (**7**), 4-NO_2-C_6H_4 (**8**), 4-CN-C_6H_4 (**9**), 3,4,5-F_3-C_6H_2 (**10**), and C_6F_5 (**11**), were synthesized by condensation reactions of 2-formylpyrrole (**1**) with the requisite substituted aryl amines, namely aniline, 2,6-dimethylaniline, 2,6-diisopropylaniline, 4-methoxyaniline, 3,4-dimethylaniline, 4-fluoroaniline, 4-nitroaniline, 4-aminobenzonitrile, 3,4,5-trifluoroaniline, and 2,3,4,5,6-pentafluoroaniline, employing standard reaction conditions (Scheme 1). The syntheses and purifications of these ligand precursors were straightforward, and those with sterically bulky and electron-donating substituents were typically obtained in good yields. However, the ligand precursors bearing electron-withdrawing groups were always obtained with unreacted starting amines and thus had to be purified by vacuum sublimation, leading to low to moderate yields. All compounds were characterized by ^1H, ^{13}C, and, in the case of fluorinated derivatives, ^{19}F NMR spectroscopies, their spectra being consistent with those reported in the literature.

Crystals suitable for single-crystal X-ray diffraction analysis were obtained for the ligand precursors **3**–**6** and **8**. The structural features of these compounds are similar to those of other previously reported iminopyrrole molecules.[5d,e,h,15,19] In fact, the crystal structure of compound **4** has been reported previously.[5h] However, a new polymorphic form was obtained in the present work when the compound was crystallized from toluene double-layered with *n*-hexane. Perspective views of the molecular structures of the ligand precursors **3**–**6** and **8** are given in Figures S1–S5 in the Supporting Information. Selected bond lengths and angles are given in the captions to these figures. Details of the crystal structure determinations are given in Table S1 in the Supporting Information.

Synthesis and characterization of iminopyrrolyl boron complexes

The organoboron compounds **13**–**21** (Scheme 2) were obtained in good to moderate yields by reactions of the corresponding iminopyrrole ligand precursors with triphenylboron.

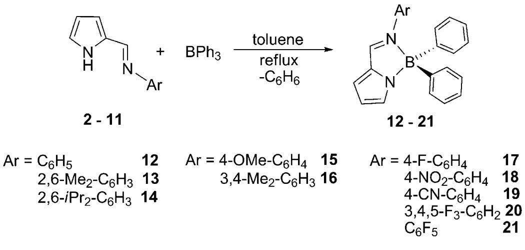

Scheme 2. Synthesis of iminopyrrolyl-BPh_2 complexes **12**–**21**.

The mixtures were heated overnight in refluxing toluene under nitrogen atmosphere. The iminopyrrolyl organoboron compounds [BPh_2{κ^2N,N'-$NC_4H_3C(H){=}N$-Ar}], with Ar = 2,6-Me_2-C_6H_3 (**13**), 2,6-*i*Pr_2-C_6H_3 (**14**), 4-OMe-C_6H_4 (**15**), 3,4-Me_2-C_6H_3 (**16**), 4-F-C_6H_4 (**17**), 4-NO_2-C_6H_4 (**18**), 4-CN-C_6H_4 (**19**), 3,4,5-F_3-C_6H_2 (**20**), and C_6F_5 (**21**), were characterized by ^1H, ^{13}C, ^{11}B, and, in the case of fluorinated compounds, ^{19}F NMR spectroscopies, as well as by elemental analysis. Where possible, single-crystal X-ray diffraction analysis was also performed. Although the organoboron compound [BPh_2{κ^2N,N'-$NC_4H_3C(H){=}N$-C_6H_5}] (**12**) has already been reported in our earlier communication,[17] it is also included in this full paper. The absence of NH proton signals in the ^1H NMR spectra of the complexes confirmed the formation of the neutral tetracoordinate boron mononuclear complexes. The ^{11}B NMR chemical shifts of these compounds are in the range $\delta = 4.88$–5.81 ppm, consistent with those of other four-coordinate boron derivatives[12] (resonances for three-coordinate boron are typically downfield shifted, appearing at $\delta \approx +25$ ppm and above[11]). In general, these iminopyrrolyl organoboron compounds could be handled in air for periods of at least an hour, but, upon prolonged exposure, underwent a relatively slow decomposition process leading to regeneration of the corresponding free ligand precursor. However, compound **21** proved to be extremely sensitive to air and moisture (in the solid state or in solution) as well as very unstable in solution even under nitrogen, undergoing very fast decomposition with concomitant regeneration of the ligand precursor. This instability, most likely due to the high electronegativity of the C_6F_5 group, could be monitored by UV/Vis absorption spectroscopy and affected the electrochemical measurements. Compounds **13**–**21** were found to be soluble in most of the common organic solvents, such as dichloromethane, tetrahydrofuran, and toluene, and moderately soluble in *n*-hexane.

Crystals suitable for X-ray diffraction analysis were obtained for compounds **13**–**17**, **19**, and **21**, enabling the determination of their crystal structures. Perspective views of the molecular structures of these iminopyrrolyl boron complexes are shown in Figure 1 (and Figure S6 in the Supporting Information) and selected bond distances and angles are given in Table 1.

In general, the boron center in each of the complexes displays a typical distorted tetrahedral geometry with *C*1 symmetry. The iminopyrrolyl ligand is chelated to the boron atom through the two nitrogen atoms to form a five-membered ring. The respective bite angles (N1-B1-N2) range from 93.81(17)° to 95.30(8)°. Throughout the series [BPh_2{κ^2N,N'-$NC_4H_3C(H){=}N$-Ar}] (**13**–**17**, **19**, and **21**), the B–C and B–N bond distances are rather invariant, with average B1–C_{ipso} and B1–N1(pyrrolyl) distances of 1.610 and 1.561 Å, respectively, the latter being shorter by 0.073 Å compared to the average B1–N2(imine) distance (1.634 Å), as previously observed for compound **12**.[17]

Furthermore, the iminopyrrolyl fragments coordinated to boron are virtually planar in all of the compounds, but the respective aryl groups bonded to the iminic nitrogen are not coplanar. The dihedral angle (defined as C6-N2-C7-C12) depends on the bulkiness of the substituents at 2,6-positions of the *N*-aryl groups. For instance, within the group of complexes bearing 2,6-substituted aryl groups (**13**, **14**, and **21**, with Me, *i*Pr and F substituents, respectively), the *N*-aryl plane is nearly perpendicular to that of the iminopyrrolyl fragment in **13** and **14**, as reflected in very high dihedral angles (81.6(3)° for **13**,

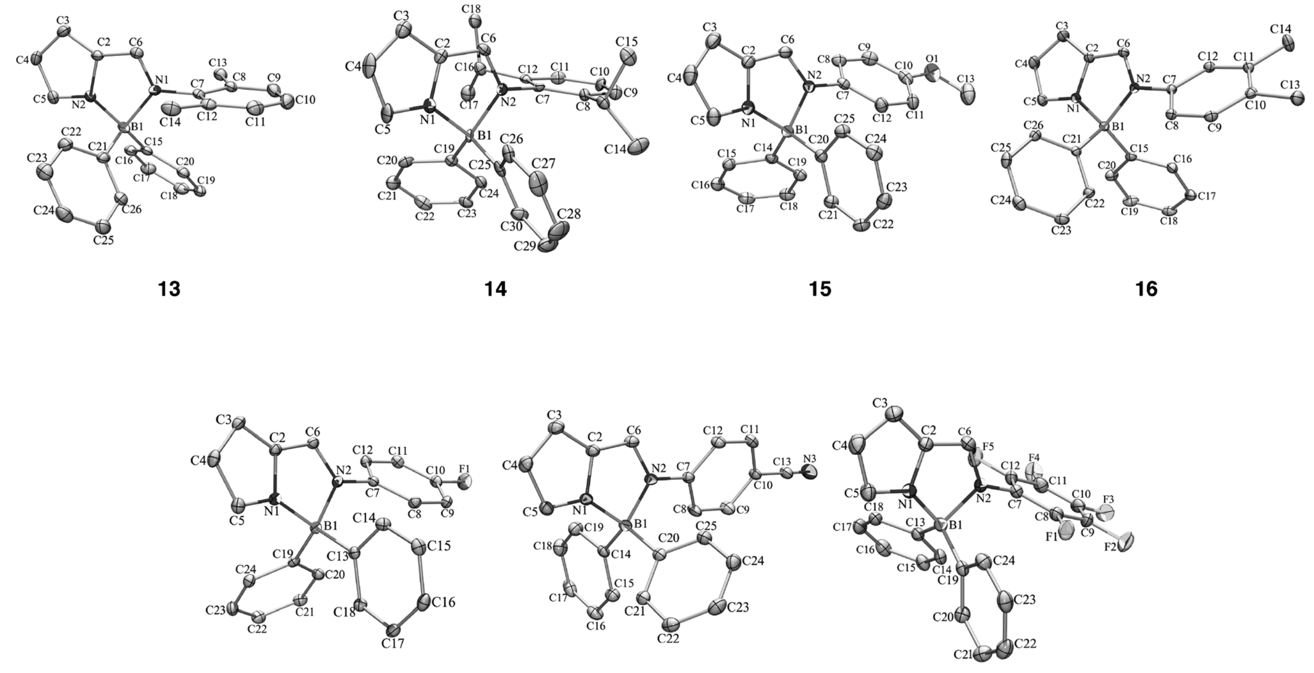

13 14 15 16

17 19 21

Figure 1. Perspective views of the molecular structures of iminopyrrolyl boron complexes **13**–**17**, **19**, and **21**. Ellipsoids are drawn at the 30 % probability level. All calculated hydrogen atoms have been omitted for clarity.

75.3(6)° for **14**). A dihedral angle of 70.3(3)° is observed for **21**, owing to the lower steric volume of the F atom compared to the Me and *i*Pr groups. In the remaining complexes **15**–**17** and **19**, in which H atoms occupy the 2,6-positions of the *N*-aryl ring, the dihedral angles are considerably smaller (41.82(19)° for **15**, 39.84(16)° for **16**, 45.7(2)° for **17**, and 27.4(2)° for **19**). The other structural features of these boron complexes resemble those of similar analogues[12a,d,17,19] and will be further discussed below, when comparing them with those of excited states.

Electrochemical properties

Cyclic voltammetry measurements on compounds **12**–**21** were performed in electrolyte solutions in dichloromethane. The respective onset oxidation and reduction potentials were used, after conversion to the absolute scale taking the Fc/Fc$^+$ (ferrocene/ferrocenium ion redox couple) as a reference, to estimate their ionization potentials (IP) and electron affinities (EA).[25] The values obtained are summarized in Table 2.

With the exception of compounds **13**, **14**, and **21**, bearing particularly twisted aryl groups owing to restricted rotation about the *N*-aryl bond, the ionization potentials are clearly correlated with the electron-donating or electron-withdrawing properties of the substituents, as represented by the sum of their classical Hammett σ constants[26] (Table 2 and Figure S7a in the Supporting Information). The electron affinities also show a correlation, although that of the strongly conjugated nitro substituent (compound **18**) falls outside the relevant trend line (Figure S7b in the Supporting Information).

Photoluminescence properties

The UV/Vis absorption and fluorescence spectra of complexes **12**–**21** in THF are shown in Figure 2 (and Figure S8 in the Supporting Information) and relevant photophysical data, listed in order of increasing absorption wavelength maxima, are summarized in Table 3. In contrast to their non-emissive ligand precursors **2**–**11**, most of the boron complexes are highly emissive in solution.

The absorption spectra show wavelength maxima (corresponding to the $S_{1,1} \leftarrow S_{0,0}$ vibronic transition) within the range 353–421 nm in THF, which depend on the steric and electronic properties of the *N*-aryl substituents. The absorption spectra of the 2,6-substituted compounds (**13**, **14**, and **21**) are considerably blue-shifted with respect to that of the unsubstituted parent compound (**12**). This feature is due to the large torsion angle between the *N*-aryl ring and the iminopyrrolyl fragment ($>70°$, see the last row of Table 1), which prevents π-conjugation (resonance) between the two fragments. On the other hand, substitution at the 3-, 4-, or 5-positions of the *N*-aryl ring leads to red-shifts of the absorption maxima, the magnitudes of which also depend on the electron-donating or electron-withdrawing properties of these substituents. The correlation of the absorption energy maxima with IP$-$EA (Table 2 and Figure S9a in the Supporting Information), which assumes proportionality between the S_0-S_1 and HOMO–LUMO energy gaps, is surprisingly good (except for compound **21**), given the absence of CIS (configuration interaction of states),[27] which is required for conversion of orbital energies into state energies.

The fluorescence emission maxima (412–505 nm) correspond to the $S_{1,0} \rightarrow S_{0,1}$ vibronic transition, except in the case of the

Table 1. Selected bond distances [Å] and angles [°] for complexes **13**–**17**, **19**, and **21**.

	13[a]	**14**[a]	**15**	**16**	**17**	**19**	**21**[a]
Distances							
N1—C2	1.376(3)	1.364(6)	1.375(2)	1.3749(15)	1.3794(19)	1.381(2)	1.381(3)
N1—C5	1.347(3)	1.356(6)	1.347(2)	1.3465(15)	1.3467(19)	1.337(2)	1.343(3)
N2—C6	1.297(3)	1.299(6)	1.304(2)	1.3083(14)	1.3172(18)	1.319(2)	1.313(3)
N2—C7	1.439(3)	1.452(6)	1.424(2)	1.4301(14)	1.4285(18)	1.426(2)	1.418(3)
N1—B1	1.561(4)	1.541(7)	1.566(2)	1.5660(15)	1.565(2)	1.569(3)	1.561(3)
N2—B1	1.645(4)	1.625(7)	1.634(2)	1.6306(16)	1.633(2)	1.630(2)	1.644(3)
C_{aryl1}—B1	1.594(4)	1.605(7)	1.618(2)	1.6206(18)	1.621(2)	1.603(3)	1.603(4)
C_{aryl2}—B1	1.615(4)	1.591(8)	1.604(2)	1.6189(16)	1.608(2)	1.613(3)	1.611(4)
X—$C_{N\text{-aryl-}p}$[b]			1.371(2)	1.5061(17)	1.3593(17)	1.439(3)	1.343(3)
Y—X—$C_{N\text{-aryl-}p}$[b,c]			1.407(2)			1.145(2)	
X—$C_{N\text{-aryl-}m}$[d]				1.5047(17)			1.342(3) 1.339(3)
X—$C_{N\text{-aryl-}o}$[e]	1.501(4) 1.496(4)	1.508(7) 1.508(7)					1.332(3) 1.347(3)
Angles							
C2-N1-C5	107.2(2)	107.1(5)	107.88(13)	107.46(9)	107.78(12)	107.70(15)	107.7(2)
C2-N1-B1	112.4(2)	112.7(4)	112.14(12)	112.00(9)	112.51(12)	112.20(14)	113.00(18)
C5-N1-B1	139.2(2)	139.1(5)	139.68(14)	140.45(10)	139.50(13)	140.05(16)	139.3(2)
C6-N2-C7	120.6(2)	119.7(4)	121.64(13)	121.03(9)	121.43(12)	122.30(15)	122.52(19)
C6-N2-B1	110.7(2)	110.9(4)	111.03(12)	110.52(9)	110.87(12)	110.76(14)	111.30(18)
C7-N2-B1	128.6(2)	128.4(4)	126.86(12)	128.28(9)	127.51(11)	126.89(14)	124.78(18)
N1-B1-N2	94.69(19)	94.9(4)	94.90(11)	95.30(8)	94.90(11)	95.35(13)	93.81(17)
C_{aryl1}-B1-C_{aryl2}	116.0(2)	114.7(5)	117.82(13)	112.91(9)	115.76(12)	118.88(16)	119.2(2)
N1-B1-C_{aryl1}	113.8(2)	108.5(4)	112.91(12)	111.61(9)	112.07(12)	110.45(15)	111.77(19)
N1-B1-C_{aryl2}	109.0(2)	115.8(5)	110.28(12)	110.72(9)	109.96(12)	108.82(15)	112.2(2)
N2-B1-C_{aryl1}	111.3(2)	111.6(4)	107.25(12)	110.07(9)	109.59(12)	111.02(14)	110.81(17)
N2-B1-C_{aryl2}	110.0(2)	109.7(4)	111.26(11)	114.99(9)	112.70(12)	110.02(14)	105.93(18)
C6-N2-C7-C12[f]	81.6(3)	75.3(6)	41.82(19)	39.84(16)	45.7(2)	27.4(2)	70.3(3)

[a] Due to the similarity of the parameters for the molecules in the asymmetric unit, only bond distances and angles for molecule A are presented. [b] X = O (**15**), C (**16**, **19**), F (**17**, **21**). [c] Y = C (**15**), F (**17**). [d] X = C (**16**), F (**17**). [e] X = C (**13**, **14**), F (**17**). [f] For molecule B, the dihedral angle C6-N2-C7-C12 is 80.9(3)° in **13**, 79.4(6)° in **14**, and 75.1(3)° in **21**.

Table 2. Ionization potentials (IP) and electron affinities (EA) of complexes **12**–**21**, estimated from cyclic voltammetry measurements, derived IP—EA values, energies of the absorption maximum (E_{abs}^{max}) and of the first vibronic transition (E_{em}^{0-0}), and the sum of Hammett σ constants of the corresponding *N*-aryl substituents.

Cmpd	*N*-aryl ring substituents	IP [eV]	EA [eV]	IP—EA [eV]	E_{abs}^{max} [eV]	E_{em}^{0-0} [eV]	$\sigma_o+\sigma_m+\sigma_p$[a]
12	none	5.64	2.82	2.82	3.24	2.75	0
13	2,6-Me_2	5.82	2.56	3.26	3.51	3.20	−0.34
14	2,6-iPr_2	5.83	2.56	3.27	3.51	3.21	−0.46
15	4-OMe	5.45	2.74	2.71	3.21	2.65	−0.29
16	3,4-Me_2	5.52	2.74	2.78	3.23	2.72	−0.02
17	4-F	5.66	2.86	2.80	3.25	2.77	0.05
18	4-NO_2	5.83	3.43	2.40	2.95	2.67	0.78
19	4-CN	5.78	3.06	2.72	3.07	2.74	0.66
20	3,4,5-F_3	5.79	2.99	2.80	3.18	2.79	0.73
21[b]	2,3,4,5,6-F_5	5.58	3.01	2.57	3.38	2.87	1.23

[a] Sum of the Hammett constants (ref. [26]). [b] Compound unstable in solution.

nitro-substituted compound **18**, for which the maximum corresponds to the $S_{1,0} \rightarrow S_{0,0}$ transition. The higher intensity of the $S_{1,0} \rightarrow S_{0,0}$ transition of **18** indicates a smaller change in the equilibrium geometries of its ground and excited states, that is, a rather planar ground-state geometry, in agreement with the lowest computationally calculated dihedral angle between the iminopyrrolyl and aryl moieties in this complex (25.07°, see Figure 3). Accordingly, compound **19**, which has the second lowest dihedral angle (25.8°), shows the second best vibrationally resolved emission (Figure 2).

As observed for their absorptions, the fluorescence of the violet-emitting 2,6-substituted *N*-aryl sterically hindered compounds **13**, **14**, and **21** is substantially shifted to shorter wavelengths with respect to that of **12**, while that of the remaining blue to blue-greenish-emitting compounds is shifted to longer wavelengths. Again, some correlation with the LUMO-HOMO energy gap is observed (Table 2 and Figure S9b in the Supporting Information), except in the cases of compounds **18** and **21**.

The fluorescence quantum yields and lifetimes are dictated by the non-radiative rate constants (k_{nr}) (the variation of the radiative rate constant k_f among all of the compounds is relatively small). The 2,6-substituted compounds **13** and **14** show the largest values of k_{nr} (ca. 10^{10} s^{-1}) and, consequently, very low fluorescence quantum yields (0.005 and 0.023). Conversely, the highest quantum yields are observed for **18**, **19**, and **20**, which show the lowest k_{nr} values (ca. 10^{8} s^{-1}). In order to clarify the origin of these differences in the k_{nr} values, triplet formation quantum yields ϕ_T were measured for **13**, **12**, and **19**, as compounds representative of high, medium, and low values of k_{nr}, respectively (Table 4).

For the 2,6-dimethyl-substituted compound **13**, no triplet formation was found, indicating that exclusively internal conversion is responsible for the non-radiative decay of the singlet excited state S_1 of this compound. The exceptionally high value of k_{ic} is also responsible for the abnormally low fluorescence quantum yield and lifetime (36 ps) of **13** within this series of compounds. For the parent (unsubstituted) compound **12**, ϕ_T is also low (ca. 1%) and internal conversion is similarly the dominant mechanism of non-radiative decay. Finally, the cyano-substituted compound **19** has a tenfold lower k_{ic} relative to **12**, most likely due to the extended π-conjugation of the cyanophenyl and iminopyrrolyl moieties, which may increase the rigidity of the complex in the S_1 excited state.

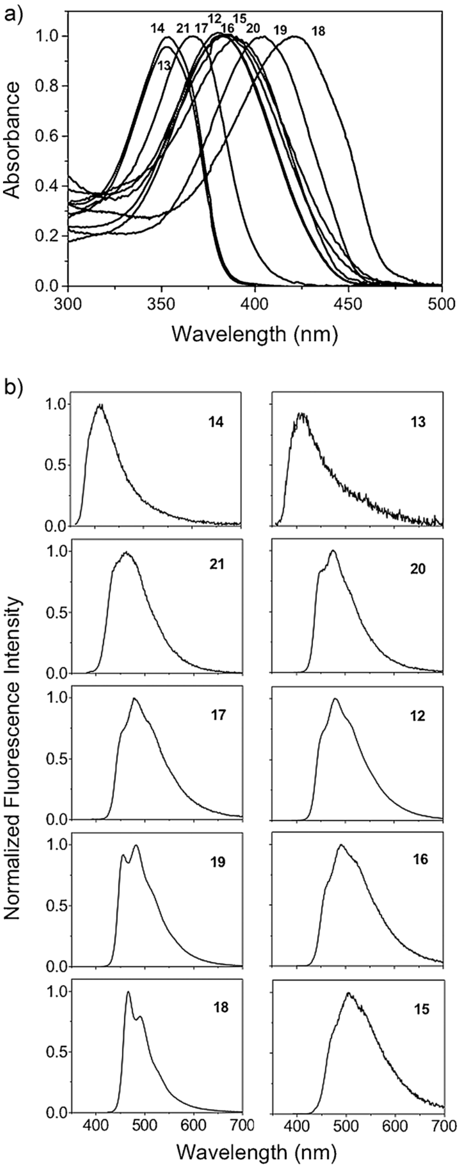

Figure 2. Normalized a) absorption and b) emission spectra of complexes **12**–**21** in THF.

It is interesting to note that, except for the compounds bearing aryl groups with substituents at the 2,6-positions, **13**, **14**, and **21**, general trends are observed for the emissions of complexes **12**–**21**: the use of increasingly electron-withdrawing *N*-aryl substituents shifts the emission wavelength maxima to higher energies and increases the fluorescence quantum yields (see Figures S10a and S10b in the Supporting Information, respectively). These electronic effects, along with the steric effect of 2,6-substitution, enable color tuning of this molecular system in the range from violet to blue to bluish-green (see Figure S11 in the Supporting Information).

Density functional calculations

DFT calculations[28] (ADF[29] program) were performed in order to understand the influence of substituents on the properties of the boron compounds **12**–**21**. The geometries of the ground state and the first excited singlet state (obtained by promoting one electron from the HOMO to the LUMO) were fully optimized. The BP86 functional and a triple-ζ basis set, as used for geometry optimization of complex **12** (only hydrogen atoms on the arene ring) and others in a previous study,[18] were also employed here in order to compare the present results with previously obtained data relating to other boron compounds. Time-dependent DFT (TD-DFT)[30] was used to obtain the absorption spectra and the lifetimes of the first excited singlet states (same functional and basis set). Some calculations were performed in the gas phase and others also in THF, as specified in the text below.

Molecular geometries

The optimized geometries of the ground states and the first excited singlet states are shown in Figure 3 (and Figure S12 in the Supporting Information), emphasizing the dihedral angle between the iminopyrrolyl and aryl moieties. The agreement between the calculated and experimental dihedral angles of the ground-state compounds is generally very good, considering that rotation about the N–C bond is essentially unhindered (Figure 3). The best agreements are observed for **19** (CN), with values of 27.4° and 25.8°, and **14**, with values of 75.3° and 74.2°. In **15**, **16**, and **17**, the deviations range from about 10 to 15°. No experimental structures could be obtained for **18** and **20**. The largest deviations are observed in **13** (Me_2) and **21** (F_5), and can probably be attributed to dimeric association of the molecules through weak C–H⋯π hydrogen bonds in the corresponding crystal structures. The aryl ring is distorted in order to maximize hydrogen bonding. This interaction energy was not calculated, since it is outside the scope of this work. For the compound with the bulkiest *ortho* substituents, **14** ($i\mathrm{Pr}_2$), a perfect agreement between the calculated and experimental dihedral angles was observed, despite also existing as a dimer. Based on the good agreement between the experimental and calculated structural parameters, we trust this methodology to provide reliable estimates of the geometrical features of compounds **18** and **20**, for which no X-ray structures are available.

Some trends are evident in these structures, namely that the dihedral angle is always higher than 25° in the ground-state structures and drops to close to zero (planar ligand) in the singlet excited states of all of the compounds, except those with two *ortho* substituents (**13** (Me_2), **14** ($i\mathrm{Pr}_2$), **21** (F_5)). As mentioned above, the reason for this is the steric hindrance of the substituents, which prevents the attainment of planarity in this state, and is reflected in the higher angles of 41.67° in **14** ($i\mathrm{Pr}_2$), 35.78° in **13** (Me_2), and 22.04° in **21** (F_5).

Interestingly, these geometrical features seem to correlate well with the low experimental fluorescence quantum yields ϕ_f (Table 3). In particular, the nonplanarity of the ligand in the singlet excited state of the hindered 2,6-substituted *N*-aryl derivatives may be associated with very low ϕ_f values of 0.005 for **13** (Me_2) and 0.023 for **14** ($i\mathrm{Pr}_2$). Compounds **15**–**20** (and also **12**[18]), with virtually planar ligands in their singlet excited states, display much higher values of ϕ_f. The ligand in the sin-

Table 3. Wavelength maximum (λ_{abs}^{max}) and molar extinction coefficient (ε_{max}) of the first absorption band, wavelength maximum (λ_{em}^{max}) and wavelength of the first vibronic transition (λ_{em}^{0-0}) of the emission band, fluorescence quantum yield (ϕ_f), fluorescence lifetime (τ_f), radiative rate constant (k_f), and sum of non-radiative rate constants (k_{nr}) of boron complexes **12**–**21** in THF at 293 K.

Cmpd	*N*-aryl ring substituents	$\Sigma\sigma_i$[a]	λ_{abs}^{max} [nm]	ε_{max} [10^4 L mol^{-1} cm^{-1}]	λ_{em}^{max} [nm]	λ_{em}^{0-0}[b] [nm]	ϕ_f	τ_f[c] [ns]	k_f[d] [ns^{-1}]	k_{nr}[e] [ns^{-1}]
14	2,6-*i*Pr$_2$	−0.46	353	1.7	412	386	0.023	0.13	0.18	7.52
13	2,6-Me$_2$	−0.34	353	1.7	413	388	0.005	0.036	0.13	27.6
21[f]	2,3,4,5,6-F$_5$	1.22	367	2.1	462	432	0.20	1.04	0.19	0.77
17	4-F	0.06	381	1.9	478	448	0.25	1.53	0.16	0.49
12[g]	none	0	383	1.7	479	451	0.34	1.90	0.18	0.35
16	3,4-Me$_2$	−0.24	384	2.0	492	456	0.14	1.22	0.11	0.70
15	4-OMe	−0.27	386	2.1	505	468	0.13	1.07	0.12	0.81
20	3,4,5-F$_3$	0.74	390	2.0	474	445	0.47	2.72	0.17	0.19
19	4-CN	0.67	404	2.2	482	453	0.71	3.28	0.22	0.09
18	4-NO$_2$	0.78	421	2.0	466	464	0.50	1.83	0.27	0.27

[a] $\Sigma\sigma_i = \sigma_o + \sigma_m + \sigma_p$ (ref. [26]). [b] From spectral decomposition with sums of four Gaussians. [c] From single exponential decays. [d] $k_f = \phi_f/\tau_f$. [e] $k_{nr} = (1-\phi_f)/\tau_f$. [f] Compound unstable in solution. [g] Ref. [17].

glet state of compound **21** is far from planar (22.04°), although less so than in **13** and **14** (35.8° and 41.7°, respectively), but its fluorescence quantum yield is higher than those of other compounds, such as **15** and **16**. In this compound, the steric effect is accompanied by the electronic effect of the five electronegative fluorine atoms, and it cannot be analyzed separately.

The energies and three-dimensional representations (Molekel[31]) of the HOMOs and LUMOs of all of the compounds (determined in THF) are shown in Figure 4 (and Figure S13 in the Supporting Information). Both the HOMO and the LUMO of all of the compounds are essentially located on the iminopyrrolyl ligand, the contribution of the aryl moiety being negligible in **14** (*i*Pr$_2$) and **13** (Me$_2$), as well as in the LUMO of **21** (F$_5$).

Electronic state transitions

The absorption maxima were calculated using the TD-DFT approach described above, both in the gas

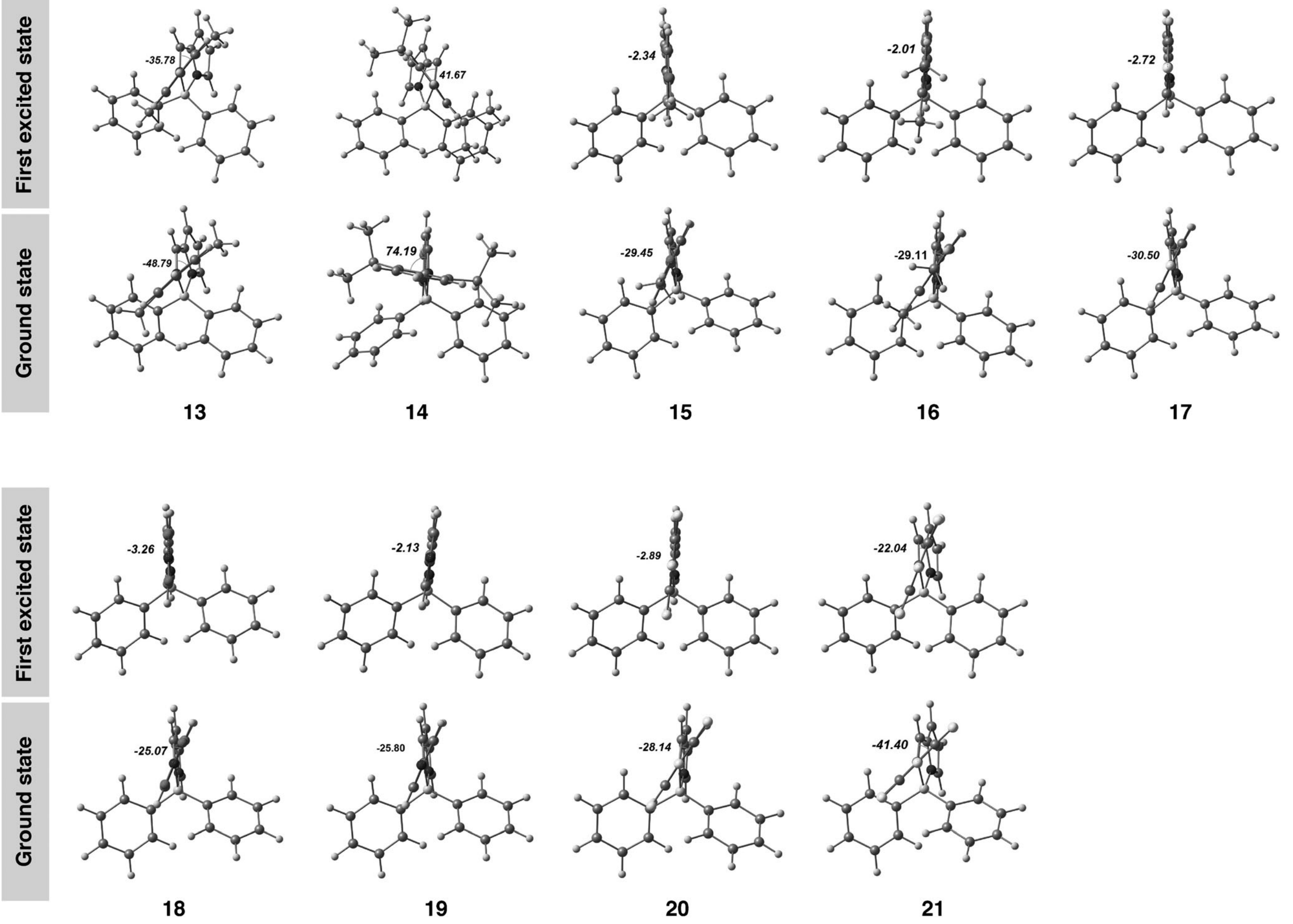

Figure 3. Optimized geometries of the iminopyrrolyl boron complexes **13**–**21** in the ground state and in the first excited singlet state, showing the dihedral angles (°).

Table 4. Fluorescence quantum yield (ϕ_f) and lifetime (τ_f), triplet formation quantum yield (ϕ_T) and lifetime (τ_T), and radiative (k_f), internal conversion (k_{ic}), and intersystem crossing (k_{isc}) rate constants of boron complexes **13**, **12**, and **19** in THF at 293 K.

Cmpd	*N*-aryl ring substituents	ϕ_f	τ_f [ns]	ϕ_T	τ_T [µs]	k_f [ns^{-1}]	k_{nr} [ns^{-1}]	k_{isc} [a] [ns^{-1}]	k_{ic} [b] [ns^{-1}]
13	2,6-Me$_2$	0.005	0.036	0	–	0.13	27.6	0.00	27.60
12	none	0.34	1.9	0.01	1.87	0.18	0.35	0.01	0.34
19	4-CN	0.71	3.28	0.2	89.5	0.22	0.09	0.06	0.03

[a] $k_{isc}=\phi_T/\tau_f$. [b] $k_{ic}=k_{nr}-k_{isc}$.

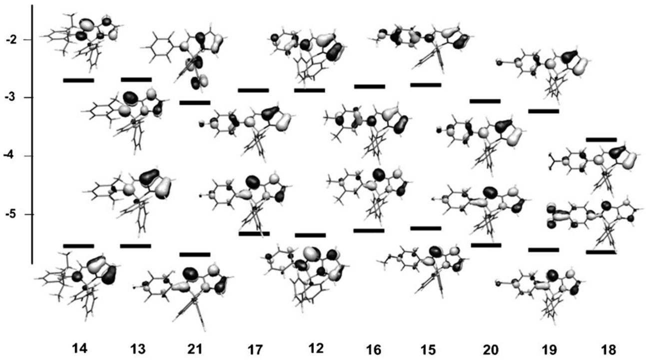

Figure 4. The energies (eV) and three-dimensional representations of the HOMOs and LUMOs (in THF) of the iminopyrrolyl boron complexes **13**–**21**.

phase (GP) and in THF, since the solvent often influences the absorption features. This methodology, however, does not allow the calculation of the radiative lifetime of the singlet excited state ($1/k_f$), which requires the introduction of spin-orbit coupling. It can be obtained from a scalar relativistic TD-DFT approach, which uses a perturbative method including the influence of spin-orbit coupling, SOPERT (SO),[32] and has been shown to yield better results when using a hybrid PBE0 functional in conjunction with an all-electron basis set (TZ2P was still used). Having performed this calculation, we used other available information on absorption spectra for comparison with our standard approach.

The calculated absorption energy maxima are given along with the experimental values in Table 5. The GP values reproduce very well the experimental values for most of the compounds, with deviations between 0 and 0.11 eV, exceptions being **14** (0.25 eV), **15** (0.25 eV), and **18** (0.35 eV). The SO values show better agreement for compound **15** (0.04 eV), but greatly overestimate the energy of the absorption maxima by a mean deviation of 0.29 eV for all the other compounds. The introduction of the solvent (THF) effect in the calculation of absorption energies also led to large deviations from the experimental values, depending on the nature of the substituents. With electronegative substituents, the calculated energies were lower than the experimental values, the largest deviations being observed for compounds **18** (NO$_2$) and **15** (OMe) (0.76 and 0.44 eV, respectively), followed by the fluorinated derivatives (**17**, **20**, **21**) with smaller deviations (0.23, 0.16, 0.20 eV). For the other species, the shifts were in the opposite direction and smaller (0.1–0.2 eV). In summary, the gas-phase values were, in general, closer to the experimental ones.

Table 5. Calculated (GP, THF, and SO) and experimental energy maxima [eV] of the lowest energy band.

Cmpd	*N*-aryl ring substituents	E_{abs}^{max}(exp) [eV]	E_{abs}^{max}(GP) [eV]	E_{abs}^{max}(THF) [eV]	E_{abs}^{max}(SO) [eV]
14	2,6-*i*Pr$_2$	3.51	3.76	3.79	3.92
13	2,6-Me$_2$	3.51	3.62	3.75	3.86
21	2,3,4,5,6-F$_5$	3.38	3.38	3.18	3.70
17	4-F	3.25	3.25	3.02	3.47
12	none	3.24	3.29	3.34	3.48
16	3,4-Me$_2$	3.23	3.16	3.17	3.41
15	4-OMe	3.21	2.96	2.77	3.25
20	3,4,5-F$_3$	3.18	3.23	3.02	3.47
19	4-CN	3.07	3.14	3.16	3.40
18	4-NO$_2$	2.95	2.60	2.19	3.24

The low-energy transition was 90% HOMO (H) to LUMO (L) for compound **12** (H), both orbitals being delocalized over the aryliminopyrrolyl moiety.[18] Two other compounds, **13** and **19**, were studied in more detail.

In **13** (2,6-Me$_2$), the low-energy band has contributions from three transitions: H-5→L (98%); H-7→L (49%)+H→L (40%); H-6→L (71%)+H→L (19%). The HOMO and LUMO are localized on the iminopyrrolyl part of the ligand, while H-5 and H-7 are essentially on the aryl ring and H-6 has some contribution from boron (see Figure 5, as well as Figure S14 in the Supporting Information). Thus, the band is characterized by significant intraligand charge transfer from the aryl to the iminopyrrolyl moiety, which may contribute to the measured low fluorescence yield (Table 3).

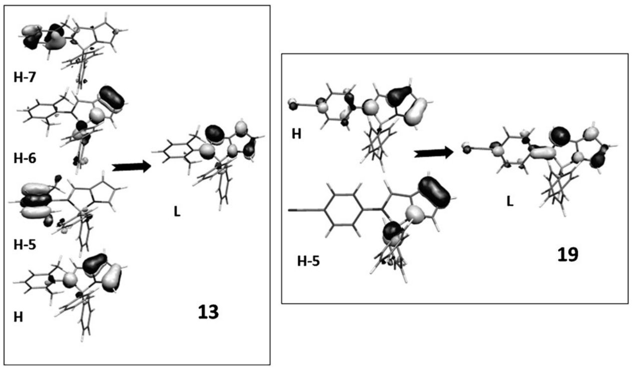

Figure 5. The nature of the transitions leading to the lower-energy absorption bands for **13** (2,6-Me$_2$) (left) and **19** (CN) (right).

In **19** (CN), the low-energy band has contributions from two transitions: H→L (84%)+H-5→L (5%); H-5→L (88%)+H→L (6%). The HOMO and LUMO are localized on the cyanoaryliminopyrrolyl ligand, while H-5 is almost completely on the pyrrolyl moiety, with a small contribution from boron (Figure 5). In this compound, the intraligand contribution of the pyrrolyl group is dominant, even compared to the unsubstituted compound **12**, which may be responsible for the increased fluorescence yield (Tables 3 and 4).

The emission wavelength was calculated from the energy difference between the excited singlet state and the ground state with the same geometry, both in the gas phase (GP) and in THF. The geometry was optimized using the standard approach in ADF (BP86 functional) as described above. Reproducing emission energies is difficult, as has been reported by other authors. Since new and (in principle) better methodologies have become available for optimizing the excited states with TD-DFT, combining several excitations and affording the emission energy directly, we thought that it would be interesting to compare them with the established approach involving only the HOMO to LUMO excitation. The radiative lifetimes ($1/k_f$) of the singlet excited states were obtained from SO calculations, as mentioned above, allowing calculation of the k_f values. All of the results are collected in Table 6 and compared with the experimental values (emission maxima).

Table 6. Calculated (GP, THF, and TD-DFT) and experimental energy maxima (E_{em}^{max}) of the emission bands and calculated (SO) and experimental fluorescence rate constants (k_f) of boron complexes **12**–**21**.

Cmpd	*N*-aryl ring substituents	E_{em}^{max}(exp) [eV]	E_{em}^{max}(GP) [eV]	E_{em}^{max}(THF) [eV]	E_{em}^{max}(TD-DFT) [eV]	k_f (exp) [ns^{-1}]	k_f (SO) [ns^{-1}]
14	2,6-*i*Pr$_2$	3.01	2.12	2.17	nc[a]	0.18	0.01
13	2,6-Me$_2$	3.00	1.97	2.02	3.02	0.13	0.13
21	2,3,4,5,6-F$_5$	2.68	2.05	2.09	nc[a]	0.19	0.004
17	4-F	2.59	1.86	1.92	3.00	0.16	0.22
12	none	2.59	1.89	1.96	2.94	0.18	0.18
16	3,4-Me$_2$	2.52	1.83	1.88	3.01	0.11	0.25
15	4-OMe	2.46	1.76	1.79	3.25	0.12	0.19
20	3,4,5-F$_3$	2.62	1.88	1.95	3.23	0.17	0.14
19	4-CN	2.57	1.87	1.95	2.73	0.22	0.08
18	4-NO$_2$	2.66	2.02	1.93	nc[a]	0.27	0.11

[a] Not converged.

The GP energy values are systematically much higher for all of the compounds, which is not surprising since they rely on a single HOMO–LUMO excitation. The solvent correction (THF values) shifts all calculated values closer to the experimental ones, but only by a small amount. For instance, the calculated emission of compound **13** (Me$_2$) is increased from 1.97 to 2.02 eV, but is still too far from the experimental value of 3.00 eV. On the other hand, the TD-DFT values reproduce the observed energies more closely, almost perfectly for **13**, but with deviations of 0.16 eV for **19** (CN) and 0.35–0.79 eV for the other compounds. Although these calculations require much longer times, the inclusion of several excitations leads to a good agreement between calculated and experimental emissions.

The calculation of emission energies is still a challenge and therefore several computational approaches must be tested. Owing to their limitations, it is not yet possible to give a simple picture of emission that has a reliable predictive capability.

The excited singlet-state lifetimes are given as fluorescence rate constants (k_f). The values are generally close to the experimental ones, with small deviations in both directions. The agreement is perfect for compounds **12** and **13**. For the compounds with π-donating substituents, such as F (**17**, **20**) or OMe (**15**), the calculated fluorescence rate constants are very close to the experimental values, whereas for those bearing π-accepting groups such as cyanide (**19**) or nitro (**18**), the agreement is poor. Compound **21**, with five electronegative F substituents, two of them in *ortho* positions, represents the largest challenge for the calculation method, and the calculated excited singlet-state lifetime was the furthest away from the experimental value.

Electroluminescence properties

Light-emitting diodes, LEDs, with the simple ITO/PEDOT:PSS/complex (**12**–**21**)/Ca/Al structure, were firstly prepared, with films of the emissive complexes being deposited by spin-coating inside a glove box. The relative positions of the frontier energy levels of the components used in the various LED structures are shown in Figure S17 in the Supporting Information. The emissions obtained from LEDs based on the complexes with the lowest solution PL quantum yields, **13** and **14** (containing 2,6-substituted *N*-aryl rings), were very dim. We could not record their electroluminescence (EL) spectra. In addition, LEDs based on the complexes with strongly electron-accepting groups (**18**, **20**, and **21**) also showed very low emission intensities, in spite of their moderate solution fluorescence quantum yields (ϕ_f). Among these, it is worth mentioning the results obtained for **18**, which showed a solution quantum yield of 50 %, yet the emission intensity of its LED was the lowest among the series. It is also interesting to note that for these complexes there is no electron-injection barrier with respect to the calcium cathode, pointing to an "excess" electron injection with respect to the hole injection from PEDOT:PSS. It is also possible that there may be significant PL quenching in the solid state compared to solution, contributing to the very poor device performance. However, LEDs based on complexes **15**, **16**, **17**, and **19** showed significant emission intensities, with **16** exhibiting a maximum luminance of 614 cd m^{-2} with a peak EL efficiency of 0.2 cd A^{-1} (see Table 7). Although **16** showed only a modest solution photoluminescence (PL) quantum yield (ϕ_f) of 14 % (see Table 3), it was the complex that performed best in this simple LED structure. From Figure S17 (Supporting Information), we conclude that, among these four complexes, **15** and **16** have similar electron- and hole-injection barriers. The difference in LED emission efficiencies may possibly result from differences in charge transport, assuming that these complexes have similar ϕ_f values in the solid state and in solution, with **16** exhibiting more equilibrated hole and electron mobilities.

Complexes **15**–**20**, those in this new series that showed the highest solution ϕ_f values, were further tested in LEDs, for which they were deposited by sublimation on top of either PEDOT:PSS or *N*,*N*′-bis(3-methylphenyl)-*N*,*N*′-diphenylbenzidine (TPD)-coated PEDOT:PSS. Barium was used as cathode material, protected with an overlayer of Al. Among the ITO/PEDOT:PSS/

Table 7. Maximum luminance (L_{max}) in [cd m^{-2}], luminous EL efficiency ($\phi_{EL,max}$) in [cd A^{-1}], and external quantum efficiency (EQE$_{max}$) in [%] of LEDs based on complexes **12**–**21**. Films were prepared by spin-coating (in the case of the Ca-based LEDs) or by sublimation.

Complex	*N*-aryl ring substituents		ITO/PEDOT:PSS/complex/Ca (spin-coating)	ITO/PEDOT:PSS/complex/Ba (sublimed)	ITO/PEDOT:PSS/TPD/complex/Ba (sublimed)
12	none	L_{max}	0.35	–	–
		$\phi_{EL,max}$	3.8×10^{-4}	–	–
		EQE$_{max}$	1.5×10^{-4}	–	–
13	2,6-Me$_2$	L_{max}	0.096	–	–
		$\phi_{EL,max}$	5.6×10^{-6}	–	–
		EQE$_{max}$	6.6×10^{-6}	–	–
14	2,6-*i*Pr$_2$	L_{max}	0.085	–	–
		$\phi_{EL,max}$	3.56×10^{-6}	–	–
		EQE$_{max}$	1.92×10^{-6}	–	–
15	4-OMe	L_{max}	31	22	500
		$\phi_{EL,max}$	0.036	0.006	0.16
		EQE$_{max}$	0.013	0.002	0.058
16	3,4-Me$_2$	L_{max}	614	755	2965
		$\phi_{EL,max}$	0.2	0.31	1.4
		EQE$_{max}$	0.079	0.12	0.48
17	4-F	L_{max}	43	53	384
		$\phi_{EL,max}$	0.005	0.03	0.22
		EQE$_{max}$	0.002	0.01	0.087
18	4-NO$_2$	L_{max}	0.066	0.28	2.1
		$\phi_{EL,max}$	2.36×10^{-5}	4.8×10^{-4}	2.85×10^{-3}
		EQE$_{max}$	8.2×10^{-6}	1.6×10^{-4}	9.9×10^{-4}
19	4-CN	L_{max}	–	80	246
		$\phi_{EL,max}$	–	0.072	0.089
		EQE$_{max}$	–	0.027	0.036
20	3,4,5-F$_3$	L_{max}	0.012	0.26	1.4
		$\phi_{EL,max}$	0.002	2.09×10^{-5}	8.5×10^{-5}
		EQE$_{max}$	0.001	8.2×10^{-6}	3.4×10^{-5}
21	2,3,4,5,6-F$_5$	L_{max}	0.28	–	–
		$\phi_{EL,max}$	6.4×10^{-5}	–	–
		EQE$_{max}$	3.3×10^{-5}	–	–

sublimed complex/Ba devices, those based on **16** showed the best performance, as found in the Ca-based LEDs, with a maximum luminance of 755 cd m^{-2} and a maximum EL efficiency of 0.31 cd A^{-1}. As observed for the first series of LEDs, those based on complexes **18** and **20** showed the poorest performances. The use of Ba in place of Ca should improve the electron-injection efficiency in the case of complexes **15**, **16**, and possibly also **17** (albeit to a lesser extent), maintaining the ohmic electron injection for the remaining complexes of the studied series. We attribute the observed differences in performance for the devices based on complexes **18**–**20** to the different film preparation processes (sublimation *vs* solution spin-coating). We consider that the variation in the performances of the devices based on complexes **15**–**17** is inconsistent with reduction of the electron-injection barrier upon the use of Ba (which should intrinsically improve the EL efficiency, but was not realized for **15**). Again, we believe that the change in the film preparation process is the main contributing factor.

The insertion of a TPD hole-transporting/electron-blocking layer (HT/EBL), with a HOMO lying slightly lower in energy than the PEDOT:PSS workfunction, should improve hole injection for all of the complexes by creating an intermediate level between the PEDOT:PSS workfunction and their HOMO levels. In addition, its high-lying LUMO prevents electrons from escaping to the PEDOT:PSS electrode, thereby improving the electron-hole recombination. In fact, we observed a significant improvement in performance of the LEDs based on these six complexes (**15**–**20**), although the devices based on **18** and **20** still showed very poor performances. Among the other LEDs, those based on **16** showed the best performance, as observed for the other device types, with a maximum luminance of nearly 3000 cd m^{-2} and a maximum EL efficiency of 1.4 cd A^{-1}. In fact, the devices based on complexes **15** and **16**, with electron-donating groups on the *N*-aryl moiety, displayed the highest luminances, in spite of the modest solution ϕ_f values (13 % and 14 %, respectively) of these complexes. LEDs based on **19**, the complex showing the highest solution ϕ_f (71 %), were not the best performing. Figure 6 (and Figure S15 in the Supporting Information) compares the performances of LEDs based on **16** and **19**, having barium cathodes, and with or without an HT/EBL made of TPD. In both cases, the insertion of TPD led to an increase in the maximum luminance and also enhanced the EL efficiency (in the case of **16**, it led to an increase in the maximum EL efficiency from 0.31 to 1.4 cd A^{-1}, whereas in the case of **19** it led to a much more modest increase from 0.07 to 0.09 cd A^{-1}). It is also interesting to note that while the solution PL efficiency of

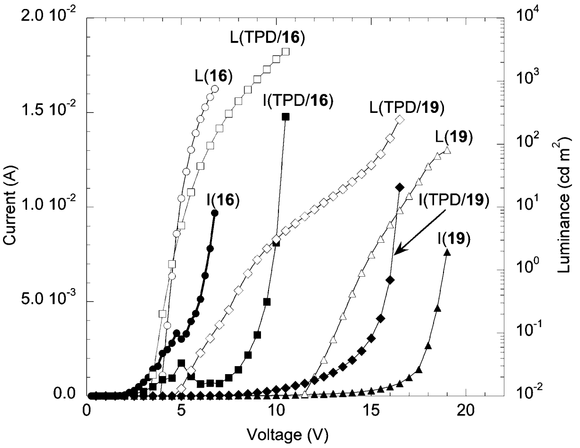

Figure 6. Current (I, filled symbols) and luminance (L, open symbols) for LEDs based on **16** (film thickness 80 nm) and **19** (film thickness 60 nm). Results are shown for ITO/PEDOT:PSS/complex/Ba/Al and ITO/PEDOT:PSS/TPD/complex/Ba/Al device structures.

19 was higher than that of **16** (71 % versus 14 %), the reverse was true for the EL efficiencies. This behavior could be due to differences in PL efficiency in the solid state (with detrimental stronger dipole interactions in the case of **19**), higher hole-injection barrier, due to a higher ionization potential of **19** with respect to that of PEDOT:PSS (5.2 eV), and possibly also differences in hole and/or electron mobilities.

From the results shown in Table 7, it can be concluded that the presence of electron-withdrawing substituents on the *N*-aryl fragment is generally detrimental to device performance. Complexes **17** and **19**, with fluoro and cyano substituents in the *para* position, respectively, show intermediate performances. With an increase in the number of groups and/or their electron-withdrawing strengths, the performance decreases even further.

Figure 7 (and also Figure S16 in the Supporting Information) compares the PL spectra of three complexes, **16** and **19** (the LED characteristics of which are shown in Figure 6) and **18**, which bears a strongly electron-withdrawing group (NO_2) and, in spite of its reasonable solution PL efficiency of 50 %, yielded poorly performing LEDs. For complex **16**, the solution and thin-film PL spectra are similar (with a red-shift of the emission maximum from 490 to 505 nm on going from solution to a thin film), with the EL spectrum having a maximum at an intermediate wavelength (Figure 7 A). The solid-state PL spectrum of complex **19** shows a significantly red-shifted maximum (516 nm) with respect to the solution PL (maximum at 482 nm), and a stronger tail at longer wavelengths (Figure 7 B). Surprisingly, the EL spectrum is not as shifted toward lower energies as the PL spectrum. This is somewhat unexpected, as we would suppose the accessible excited states to be the same under both photo and electrical excitation. We do not yet have a definitive explanation for this observation as, in view of the spectral shapes, interference effects are unlikely to be the cause. For complex **18**, the red-shift of the thin-film PL spectrum with respect to that obtained from the solution is even more pronounced, with the maximum increasing from about 466 nm to 524 nm (Figure 7 C). This effect, combined with the loss of vibronic resolution, indicates that a different lowest-energy state appears in the solid state, which is most likely of intermolecular origin. The emission of the **18**-based LEDs was too weak to allow us to record an EL spectrum, which indicates that, in spite of the high solution PL efficiency of 50 %, the lowest-energy state formed in the solid state has insufficient emission efficiency.

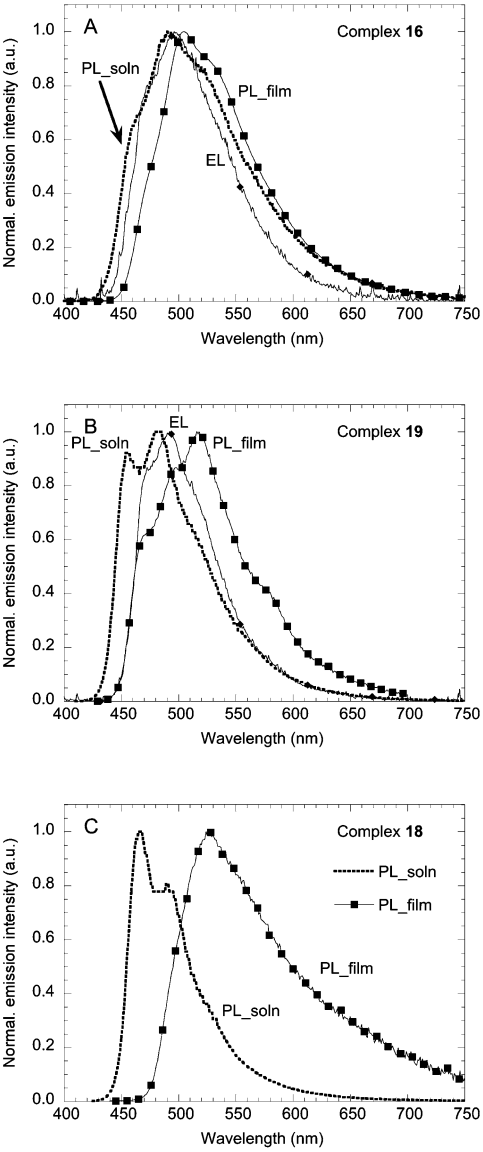

Figure 7. Comparison of emission spectra (PL recorded in solution and from thin films, and EL of the thin films) for complexes (A) **16**, (B) **19**, and (C) **18**.

Conclusion

Several tetracoordinate mononuclear organoboron complexes containing 2-(*N*-arylformimino)pyrrolyl ligands with *N*-aryl ring substituents of different electronic and steric natures have been synthesized and characterized by multiple methods. X-ray crystallography studies have confirmed chelation of these ligands to the Lewis acidic diphenylboron moiety. The resulting complexes have a pseudo-tetrahedral geometry about the boron atoms, and the dihedral angle between the *N*-aryl plane and the iminopyrrolyl fragment depends upon the bulkiness of the substituents in the 2,6-positions of the aryl groups. It was found that the electronic properties of these fluorescent compounds could be varied in a predictable manner by changing the electron-donating or electron-withdrawing character of the aniline substituents. For instance, the color of emission could be tuned from blue to bluish-green by increasing the electron-donating strength of the substituents. This change was at the expense of the fluorescence quantum yield. DFT calculations have shown the geometry of the iminopyrrolyl ligand in the excited singlet state to be almost planar, except when *ortho* substituents are present, in contrast to the nonplanar ground-state structure. The low-energy band leading to emission is essentially a HOMO to LUMO transition. The more delocalized frontier orbitals seem to be associated with higher fluorescence quantum yield, whereas the introduction of some charge transfer between the ligands has the opposite effect. DFT methods lead to very good estimates of the absorption maxima, but emission is more difficult to predict, even by using the more recent methodologies. Single-layer devices, with a PEDOT:PSS hole-injection layer, have been fabricated with the prepared complexes as emissive layers, films of which were prepared either by spin-coating from solution or by sublimation. As expected, the complexes that showed the lowest solution photoluminescence (PL) efficiencies (**12**, **13**, **14**, and **21**) yielded very poorly emissive devices, and LEDs based on **18**, which has a solution PL efficiency of 50%, also showed very poor performance. The best performing devices were obtained with **16**, even though it has only a modest solution PL efficiency of 14%. Upon insertion of a hole-transporting/electron-blocking layer of TPD, the performance was greatly improved, with the devices based on **16** showing a maximum luminance of 2965 $cd\,m^{-2}$ with a maximum EL efficiency of 1.4 $cd\,A^{-1}$.

Experimental Section

General procedures

All experiments involving air- and/or moisture-sensitive materials were carried out under inert atmosphere using a dual vacuum/nitrogen line and standard Schlenk techniques. Nitrogen gas was supplied in cylinders (Air Liquide) and purified by passage through 4 Å molecular sieves. Unless otherwise stated, all reagents were purchased from commercial suppliers (e.g., Acros, Aldrich, Fluka) and used without further purification. All solvents to be used under inert atmosphere were thoroughly deoxygenated and dehydrated before use. They were dried and purified by refluxing over a suitable drying agent followed by distillation under nitrogen. The following drying agents were used: sodium (for toluene, diethyl ether, and tetrahydrofuran (THF)) and calcium hydride (for *n*-hexane and dichloromethane). Solvents and solutions were transferred using a positive pressure of nitrogen through stainless steel cannulae and mixtures were filtered in a similar way using modified cannulae that could be fitted with glass fiber filter disks.

Nuclear magnetic resonance (NMR) spectra were recorded on a Bruker Avance III 300 (^{1}H, ^{13}C, ^{11}B, and ^{19}F) spectrometer. Deuterated solvents were dried by storage over 4 Å molecular sieves and degassed by the freeze-pump-thaw method. Spectra were referenced internally to residual protio-solvent (^{1}H) or solvent (^{13}C) resonances and are reported relative to tetramethylsilane ($\delta = 0$). ^{11}B and ^{19}F NMR spectra were referenced to $Et_2O{\cdot}BF_3$ and $CFCl_3$, respectively. All chemical shifts are quoted in δ (ppm) and coupling constants are given in Hz. Multiplicities are abbreviated as follows: broad (br), singlet (s), doublet (d), triplet (t), quartet (q), heptet (h), and multiplet (m). For air- and/or moisture-sensitive materials, samples were prepared in J. Young NMR tubes in a glovebox. Elemental analyses were obtained from the IST elemental analysis service.

General method for the synthesis of iminopyrrole ligand precursors

This synthetic procedure was based on other similar methods described in the literature.[5d,19–24] In a typical experiment, an equimolar ratio of 2-formylpyrrole and a substituted aniline, a catalytic amount of *p*-toluenesulfonic acid, and $MgSO_4$ (to remove any water from the reaction mixture) were suspended in absolute ethanol (20 mL) in a round-bottomed flask fitted with a condenser and a $CaCl_2$ guard tube. The mixture was heated to reflux overnight, whereupon it turned yellow-orange. It was then allowed to cool, CH_2Cl_2 was added, and the suspension was filtered through Celite and washed through with more CH_2Cl_2. After removal of all volatiles from the filtrate in vacuo, the product was dissolved in refluxing *n*-hexane. The dark-brown oil was separated from the supernatant orange solution, and the latter was stored at −20 °C to yield orange-yellow crystals of the iminopyrrole ligand precursor. For further details of the experimental procedure and product characterization, see the Supporting Information.

General procedure for the syntheses of diphenylboron derivatives, $[BPh_2\{\kappa^2 N,N'\text{-}NC_4H_3C(H){=}N\text{-}Ar\}]$ (13–21)

In a typical experiment, an equimolar mixture of triphenylboron and the requisite iminopyrrolyl ligand precursor in toluene (15–25 mL) was stirred and heated at reflux, under nitrogen atmosphere, overnight. The reaction mixture was allowed to cool to room temperature, then concentrated under vacuum to a volume of 5 mL and double-layered with hexane. The resulting solution was kept at −20 °C to afford the corresponding crystalline boron complex. For further details of the experimental procedure and product characterization, see the Supporting Information.

X-ray data collection

Crystallographic and experimental details of the crystal structure determinations are listed in Tables S1 and S2 in the Supporting Information. The crystals were selected under an inert atmosphere, covered with polyfluoroether oil, and mounted on a nylon loop. Crystallographic data for compounds **3**–**6**, **8**, **13**–**17**, **19**, and **21** were collected at 150 K using graphite-monochromated $Mo_{K\alpha}$ radiation ($\lambda = 0.71073$ Å) on a Bruker AXS-Kappa APEX II diffractometer equipped with an Oxford Cryosystems open-flow nitrogen cryostat. Cell parameters were retrieved using Bruker SMART[33] software and refined using Bruker SAINT[34] on all observed reflections. Absorption corrections were applied using SADABS.[35] Structure solution and refinement were performed by direct methods with the programs SIR2004[36] and SHELXL[37] included in the package of programs WINGX-Version 1.80.05.[38] Except for the NH hydrogen atoms in the compounds, all hydrogen atoms were inserted in idealized positions and allowed to refine riding on the parent carbon atom. Graphic representations were prepared with ORTEP-III.[39] Data have been deposited with the CCDC under deposition numbers CCDC-957737 for **3**, 957738 for **4**, 957739 for **5**, 957740 for **6**, 957741 for **8**, 957742 for **13**, 957743 for **14**, 957744 for **15**, 957745 for **16**, 957746 for **17**, 957747 for **19**, and 957748 for **21**. CCDC-957737–957748 contain the supplementary crystallographic data for this paper. These data can be obtained free of charge from The Cambridge Crystallographic Data Centre via www.ccdc.cam.ac.uk/data_request/cif.

Cyclic voltammetry studies

Cyclic voltammetry measurements were carried out with a Solartron potentiostat using a standard three-electrode cell, with a saturated calomel reference electrode, a platinum wire as counter electrode, and a platinum disk as working electrode. The compounds were dissolved in freshly distilled dichloromethane containing 0.2 M electrolyte salt (tetrabutylammonium tetrafluoroborate or tetrabutylammonium perchlorate).

Ionization potential (IP) and electron affinity (EA) values were estimated from the onset of oxidation and reduction potentials, respectively. To convert the values on the electrochemical scale to an absolute scale, referred to the vacuum, we used ferrocene as a reference and considered the energy level of ferrocene/ferrocenium (Fc/Fc^+) to be 4.80 eV below the vacuum level, as detailed in ref. [17].

Spectroscopic measurements

Absorption and fluorescence spectra were measured on a Beckman DU-70 spectrophotometer and a SPEX Fluorolog 212I, respectively. The fluorescence spectra were collected with right-angle geometry, in the S/R mode, and corrected for instrumental wavelength dependence.

Fluorescence decays were measured using the time-correlated single-photon counting (TCSPC) technique as previously described.[40] The pulsed (82 MHz) excitation source was a Ti:sapphire Tsunami laser pumped with a Millennia Xs solid-state laser (Spectra Physics). Decays longer than 2 ns were remeasured at reduced repetition rate (4 MHz) using a pulse picker (Spectra Physics, Model 3980). The Tsunami output (720–900 nm) was frequency-doubled and vertically polarized. The sample emission was passed through a polarizer set at the magic angle and a Jobin–Yvon H10 monochromator, and finally detected with a microchannel plate photomultiplier (Hamamatsu, R3809u-50 MCP-PT). A fraction of the Tsunami output was detected with a PHD-400-N photodiode (Becker and Hickl, GmbH) for generation of the start signal. Start and stop signals were processed with an SPC-630 acquisition board (Becker and Hickl, GmbH). The instrumental response function (IRF) was measured using a LUDOX scattering solution in water with transmittance at the excitation wavelength matched to that of the sample (FWHM = 19 ps). The IRF and sample signals were collected until 5×10^3 counts at the maximum were reached. Fluorescence decays were deconvoluted from the IRF using the modulation functions method (Sand program).[41]

Flash photolysis

Triplet-state absorption spectra and quantum yields were measured with a laser flash photolysis apparatus (Applied Photophysics) pumped by an Nd:YAG laser (Spectra Physics). Transient spectra were obtained by monitoring the optical density (OD) change at intervals of 10 nm over the range 300–700 nm and averaging at least ten decays at each wavelength. Second-order kinetics was observed for the decay of the lowest triplet state. Excitation was at 355 nm with an unfocused beam. Special care was taken in determining triplet yields to have optically matched dilute solutions (abs ≈ 0.2–0.3 in a 10 mm square cell) and low laser energy (2 mJ) to avoid multiphoton and triplet-triplet (T-T) annihilation effects. The triplet molar absorption coefficients were determined by the singlet depletion technique, according to the well-known relationship:

$$\varepsilon_T = \frac{(\varepsilon_S)(\Delta OD_T)}{(\Delta OD_S)} \qquad (1)$$

where both ΔOD_S and ΔOD_T were obtained from the triplet transient absorption spectra. Triplet formation quantum yields were derived from these and actinometry with benzophenone. The intersystem-crossing yields (ϕ_T) for the compounds were obtained by comparing the ΔOD at 530 nm of solutions of benzophenone in benzene (standard) optically matched (at the laser excitation wavelength) with that of the compound using the following equation:

$$\phi_T^{\text{sample}} = \frac{\varepsilon_{TT}^{\text{benzophenone}}}{\varepsilon_{TT}^{\text{sample}}} \frac{\Delta OD_{\max}^{\text{sample}}}{\Delta OD_{\max}^{\text{benzophenone}}} \phi_T^{\text{benzophenone}} \qquad (2)$$

with $\varepsilon_{TT}^{\text{benzophenone}} = 7200\ \text{M}^{-1}\,\text{cm}^{-1}$ and $\phi_T^{\text{benzophenone}} = 1$.

Computational studies

Density functional theory calculations[28] were performed using the Amsterdam density functional program package (ADF).[29] Gradient-corrected geometry optimizations,[42] without symmetry constraints, were performed using the local density approximation of the correlation energy (Vosko–Wilk–Nusair),[43] and the generalized gradient approximation (Becke's[44] exchange and Perdew's[45] correlation functionals). Relativistic effects were treated with the ZORA approximation.[46] Unrestricted calculations were performed for excited singlet states. The core orbitals were frozen for B, C, and N (1s). Triple-ζ Slater-type orbitals (STO) were used to describe the valence shells of B, C, and N (2s and 2p). A set of two polarization functions was added to B, C, and N (single-ζ, 3d, 4f). Triple-ζ Slater-type orbitals (STO) were used to describe the valence shells of H (1s), augmented with two polarization functions (single-ζ 2s, 2p). Time-dependent DFT calculations in the ADF implementation were performed to determine the excitation energies.[30] The solvent effect was included with the COSMO approach in ADF in single-point calculations on the optimized geometries. The geometry of the excited state was calculated by promoting one electron from the HOMO to the LUMO with $S=0$. The perturbative method in the time-dependent density functional theory (TD-DFT) formalism, with the influence of spin-orbit coupling effect (SOPERT),[32] was used to calculate the excited-state lifetimes. In these calculations, complete basis sets were used for all elements (as above, but without any frozen cores) with the hybrid PBE0 functional.[47] We checked that the absorption spectra calculated by this approach were the same as those obtained under the same conditions but without including spin-orbit coupling since all the atoms are light. TD-DFT optimizations of the first singlet excited state were also performed, using the Gaussian 09 software,[48] for technical reasons, with the PBE0 functional[47] and a 6–31G** basis set for all atoms.[49]

The structures were modeled on those of compounds **13**–**17**, **19**, and **21** described above. Three-dimensional representations of the orbitals were obtained with Molekel[31] and electronic spectra with Chemcraft.[50]

Light-emitting diode studies

Light-emitting diodes were fabricated on glass/ITO substrates (ITO = indium tin oxide), which were cleaned with detergent, distilled water, acetone, and isopropanol. They were treated with oxygen plasma, prior to the deposition of PEDOT:PSS (poly(3,4-ethylenedioxythiophene) doped with polystyrene sulfonic acid, CLEVIOS P VP.AI 4083 from Heraeus Clevios GmbH) by spin-coating. The PEDOT:PSS films (40 nm thick, as measured with a DEKTAK profilometer) were annealed in air for 2 min at 120 °C, and then transferred to a nitrogen-filled glove box. Some devices were prepared with an approximately 20 nm thick, hole-transporting/electron-blocking layer of TPD (*N*,*N*′-bis(3-methylphenyl)-*N*,*N*′-diphenylbenzidine, from Aldrich), which was thermally deposited on top of the PEDOT:PSS.

Films of the complexes **12**–**21** were deposited on top of the PEDOT:PSS by spin-coating from solutions in THF, inside the glove box. The thicknesses of the films of the complexes were in the range 60–100 nm. The substrates were then placed inside an evaporation chamber, and the top metal cathode (calcium), about 40 nm thick, was deposited at a base pressure of 2×10^{-6} mbar through a shadow mask, defining pixel areas of 4 mm^2. A protecting, approximately 60 nm thick, aluminum layer was deposited on top. Alternatively, films of complexes **15**–**20** (with thicknesses ranging from 50 to 115 nm) were prepared by thermal deposition on top of either PEDOT:PSS or TPD-coated PEDOT:PSS. Device structures were completed by the deposition of barium (ca. 40 nm thick) protected by an overlayer of aluminum (ca. 60 nm thick).

Devices were tested under vacuum using a K2400 Source Meter and a calibrated silicon photodiode, as described previously.[51] Electroluminescence (EL) spectra were obtained with a CCD spectrograph (from Ocean Optics or from ScanSci). External quantum efficiencies were estimated as detailed in ref. [51].

Acknowledgements

We thank the Fundação para a Ciência e Tecnologia, Portugal, for financial support (Projects PTDC/QUI/65474/2006, PEst-OE/QUI/UI0100/2013, PEst-OE/QUI/UI0612/2013, and PEst-OE/EEI/LA0008/2013) and for fellowships to D.S., P.S.L., B.F., C.A.F., and C.S.B.G. (SFRH/BPD/47853/2008, SFRH/BD/88639/2012, SFRH/BD/80122/2011, SFRH/BD/47730/2008, and SFRH/BPD/64423/2009, respectively).

Keywords: boranes · fluorescence · *N*-iminopyrrolyl ligands · OLEDs · density functional calculations

[1] a) G. Parshall, S. Ittel, *Homogeneous Catalysis: The Applications of Chemistry of Catalysis by Soluble Transition Metal Complexes*, 2nd ed., Wiley, New York, **1992**; b) B. Cornils, W. A. Herrmann, *Applied Homogeneous Catalysis with Organometallic Compounds*, 2nd ed., Wiley-VCH, Weinheim, **2002**.

[2] K. Mashima, H. Tsuguri, *J. Organomet. Chem.* **2005**, *690*, 4414 – 4423, and references therein.

[3] T. Li, J. Jenter, P. W. Roesky, *Z. Anorg. Allg. Chem.* **2010**, *636*, 2148 – 2155.

[4] R. H. Holm, A. Chakravorty, L. J. Theriot, *Inorg. Chem.* **1966**, *5*, 625 – 635.

[5] See, for instance: a) T. K. Panda, K. Yamamoto, K. Yamamoto, H. Kaneko, Y. Yang, H. Tsurugi, K. Mashima, *Organometallics* **2012**, *31*, 2268 – 2274; b) J.-S. Mu, Y.-X. Wang, B.-X. Li, Y.-S. Li, *Dalton Trans.* **2011**, *40*, 3490 – 3497; c) H. Tsurugi, Y. Matsuo, K. Mashima, *J. Mol. Catal. A* **2006**, *254*, 131 – 137; d) R. M. Bellabarba, P. T. Gomes, S. I. Pascu, *Dalton Trans.* **2003**, 4431 – 4436; e) S. A. Carabineiro, L. C. Silva, P. T. Gomes, L. C. J. Pereira, L. F. Veiros, S. I. Pascu, M. T. Duarte, S. Namorado, R. T. Henriques, *Inorg. Chem.* **2007**, *46*, 6880 – 6890; f) S. A. Carabineiro, P. T. Gomes, L. F. Veiros, C. Freire, L. C. J. Pereira, R. T. Henriques, J. E. Warren, S. I. Pascu, *Dalton Trans.* **2007**, 5460 – 5470; g) S. A. Carabineiro, R. M. Bellabarba, P. T. Gomes, S. I. Pascu, L. F. Veiros, C. Freire, L. C. J. Pereira, R. T. Henriques, M. C. Oliveira, J. E. Warren, *Inorg. Chem.* **2008**, *47*, 8896 – 8911; h) C. S. B. Gomes, D. Suresh, P. T. Gomes, L. F. Veiros, M. T. Duarte, T. G. Nunes, M. C. Oliveira, *Dalton Trans.* **2010**, *39*, 736 – 748; i) C. S. B. Gomes, S. A. Carabineiro, P. T. Gomes, M. T. Duarte, *Inorg. Chim. Acta* **2011**, *367*, 151 – 157.

[6] a) G. J. P. Britovsek, V. C. Gibson, D. F. Wass, *Angew. Chem.* **1999**, *111*, 448 – 468; *Angew. Chem. Int. Ed.* **1999**, *38*, 428 – 447 and references therein; b) V. C. Gibson, S. K. Spitzmesser, *Chem. Rev.* **2003**, *103*, 283 – 313 and references therein.

[7] a) T. K. S. Wong, *Handbook of Organic Electronics and Photonics, Vol. 2* (Ed.: H. S. Nalwa), American Scientific Publishers, Stevenson Ranch, CA, **2008**, pp. 413 – 472; b) C. H. Chen, J. Shi, *Coord. Chem. Rev.* **1998**, *171*, 161 – 174; c) S. Wang, *Coord. Chem. Rev.* **2001**, *215*, 79 – 98.

[8] a) Z. Shen, P. E. Burrows, V. Bulovic, S. R. Borrest, M. E. Thompson, *Science* **1997**, *276*, 2009 – 2011; b) H. Aziz, Z. D. Popovic, N.-X. Hu, A.-M. Hor, G. Xu, *Science* **1999**, *283*, 1900 – 1902; c) Y. Li, Y. Liu, W. Bu, J. Guo, Y. Wang, *Chem. Commun.* **2000**, 1551 – 1552; d) S. Lamansky, P. Djurovich, D. Murphy, F. Abdel-Razzaq, H. E. Lee, C. Adachi, P. E. Burrows, S. R. Forrest, M. E. Thompson, *J. Am. Chem. Soc.* **2001**, *123*, 4304 – 4312.

[9] a) J. M. Fernández-Hernández, C.-H. Yang, J. I. Beltran, V. Lemaur, F. Polo, R. Frohlich, J. Cornil, L. De Cola, *J. Am. Chem. Soc.* **2011**, *133*, 10543 – 10548; b) C.-H. Yang, Y.-M. Cheng, Y. Chi, C.-J. Hsu, F.-C. Fang, K.-T. Wong, P.-T. Chou, C.-H. Chang, M.-H. Tsai, C.-C. Wu, *Angew. Chem.* **2007**, *119*, 2470 – 2473; *Angew. Chem. Int. Ed.* **2007**, *46*, 2418 – 2421; c) L. He, L. Duan, J. Qiao, D. Zhang, L. Wang, Y. Qiu, *Org. Electron.* **2010**, *11*, 1185 – 1191.

[10] a) J. Kavitha, S. Y. Chang, Y. Chi, J. K. Yu, Y. H. Hu, P. T. Chou, S. M. Peng, A. J. Carty, *Adv. Funct. Mater.* **2005**, *15*, 223 – 229; b) X. Yang, Z. Wang, S. Madakuni, J. Li, G. E. Jabbour, *Adv. Mater.* **2008**, *20*, 2405 – 2409; c) M. A. Baldo, D. F. O'Brien, Y. You, A. Shoustikov, S. Sibley, M. E. Thompson, S. R. Forrest, *Nature* **1998**, *395*, 151 – 154.

[11] a) Z. M. Hudson, S. Wang, *Acc. Chem. Res.* **2009**, *42*, 1584 – 1596; b) P. Chen, R. A. Lalancette, F. Jäkle, *Angew. Chem.* **2012**, *124*, 8118 – 8122; *Angew. Chem. Int. Ed.* **2012**, *51*, 7994 – 7998; c) M. Halik, W. Wenseleers, C. Grasso, F. Stellacci, E. Zojer, S. Barlow, J. L. Bredas, J. W. Perry, S. R. Marder, *Chem. Commun.* **2003**, 1490 – 1491; d) C. D. Entwistle, T. B. Marder, *Chem. Mater.* **2004**, *16*, 4574 – 4585; e) C. D. Entwistle, T. B. Marder, *Angew. Chem.* **2002**, *114*, 3051 – 3056; *Angew. Chem. Int. Ed.* **2002**, *41*, 2927 – 2931; f) R. Bernard, D. Cornu, J. P. Scharff, R. Chiriac, P. Miele, *Inorg. Chem.* **2006**, *45*, 8743 – 8748; g) R. Bernard, D. Cornu, P. L. Baldeck, J. Caslavsky, J. M. Letoffe, J. P. Scharff, P. Miele, *Dalton Trans.* **2005**, 3065 – 3071; h) F. Jäkle, *Chem. Rev.* **2010**, *110*, 3985 – 4022.

[12] a) Q.-D. Liu, M. S. Mudadu, R. Thummel, Y. Tao, S. Wang, *Adv. Funct. Mater.* **2005**, *15*, 143 – 154; b) H. Amarne, C. Baik, S. K. Murphy, S. Wang, *Chem. Eur. J.* **2010**, *16*, 4750 – 4761; c) S. Kappaun, S. Rentenberger, A. Pogantsch, E. Zojer, K. Mereiter, G. Trimmel, R. Saf, K. C. Möller, F. Stelzer, C. Slugovc, *Chem. Mater.* **2006**, *18*, 3539 – 3547; d) B. J. Liddle, R. M. Silva, T. J. Morin, F. P. Macedo, R. Shukla, S. V. Lindeman, J. R. Gardinier, *J. Org. Chem.* **2007**, *72*, 5637 – 5646; e) Y. Liu, J. Guo, H. Zhang, Y. Wang, *Angew. Chem.* **2002**, *114*, 190 – 192; *Angew. Chem. Int. Ed.* **2002**, *41*, 182 – 184; f) Z. Zhang, H. Bi, Y. Zhang, D. Yao, H. Gao, Y. Fan, H. Zhang, Y. Wang, Z. Chen, D. Ma, *Inorg. Chem.* **2009**, *48*, 7230 – 7236; g) D. Li, Z. Zhang, S. Zhao, Y. Wang, H. Zhang, *Dalton Trans.* **2011**, *40*, 1279 – 1285; h) D. Li, Y. Yuan, H. Bi, D. Yao, X. Zhao, W. Tian, Y. Wang, H. Zhang, *Inorg. Chem.* **2011**, *50*, 4825 – 4831; i) C.-C. Cheng, W.-S. Yu, P.-T. Chou, S.-M. Peng, G.-H. Lee, P.-C. Wu, Y.-H. Song, Y. Chi, *Chem. Commun.* **2003**, 2628 – 2629; j) J. Ugolotti, S. Hellstrom, G. J. P. Britovsek, T. S. Jones, P. Hunt, A. J. P. White, *Dalton Trans.* **2007**, 1425 – 1432; k) J. Yoshino, A. Furuta, T. Kambe, H. Itoi, N. Kano, T. Kawashima, Y. Ito, M. Asashima, *Chem. Eur. J.* **2010**, *16*, 5026 – 5035; l) N. Kano, A. Furuta, T. Kambe, J. Yoshino, Y. Shibata, T. Kawashima, N. Mizorogi, S. Nagase, *Eur. J. Inorg. Chem.* **2012**, 1584 – 1587; m) J. Yoshino, N. Kano, T. Kawashima, *Chem. Commun.* **2007**, 559 – 561; n) P. T. Gomes, D. Suresh, C. S. B. Gomes, P. S. Lopes, C. A. Figueira (IST), World Patent WO2013039413, **2013**; o) D. Suresh, P. T. Gomes in *Advances in Organometallic Chemistry and Catalysis: The Silver/Gold Jubilee International Conference on Organometallic Chemistry Celebratory Book*, 1st ed. (Ed.: A. J. L. Pombeiro), John Wiley & Sons, Hoboken, **2014**, Chap. 36, pp. 485-492; p) D. Li, H. Zhang, Y. Wang, *Chem. Soc. Rev.* **2013**, *42*, 8416 – 8433.

[13] a) S. Sole, F. P. Gabbai, *Chem. Commun.* **2004**, 1284 – 1285; b) W. Yang, H. He, D. G. Drueckhammer, *Angew. Chem.* **2001**, *113*, 1764 – 1768; *Angew. Chem. Int. Ed.* **2001**, *40*, 1714 – 1718; c) J. Killoran, L. Allen, J. F. Gallagher, W. M. Gallagher, D. F. O'Shea, *Chem. Commun.* **2002**, 1862 – 1863; d) Z. Q. Liu, Q. Fang, D. Wang, G. Xue, W. T. Yu, Z. S. Shao, H. M. Jiang, *Chem. Commun.* **2002**, 2900 – 2901; e) S. Yamaguchi, T. Shirasaka, S. Akiyama, K. Tamao, *J. Am. Chem. Soc.* **2002**, *124*, 8816 – 8817.

[14] a) S. L. Hellstrom, J. Ugolotti, G. J. P. Britovsek, T. S. Jones, A. J. P. White, *New J. Chem.* **2008**, *32*, 1379 – 1387; b) T.-R. Chen, R.-H. Chien, M.-S. Jan, A. Yeh, J.-D. Chen, *J. Organomet. Chem.* **2006**, *691*, 799 – 804; c) K. Rurack, M. Kollmannsberger, J. Daub, *Angew. Chem.* **2001**, *113*, 396 – 399; *Angew. Chem. Int. Ed.* **2001**, *40*, 385 – 387.

[15] C. S. B. Gomes, P. T. Gomes, R. E. Di Paolo, A. L. Maçanita, M. T. Duarte, M. J. Calhorda, *Inorg. Chem.* **2009**, *48*, 11176 – 11186.

[16] M. G. Crestani, G. F. Manbeck, W. W. Brennessel, T. M. McCormick, R. Eisenberg, *Inorg. Chem.* **2011**, *50*, 7172 – 7188.

[17] a) D. Suresh, C. S. B. Gomes, P. T. Gomes, R. E. Di Paolo, A. L. Maçanita, M. J. Calhorda, A. Charas, J. Morgado, M. T. Duarte, *Dalton Trans.* **2012**,

41, 8502–8505; and the following two errata: b) D. Suresh, C. S. B. Gomes, P. T. Gomes, R. E. Di Paolo, A. L. Maçanita, M. J. Calhorda, A. Charas, J. Morgado, M. T. Duarte, *Dalton Trans.* **2012**, *41*, 14713; c) D. Suresh, C. S. B. Gomes, P. T. Gomes, R. E. Di Paolo, A. L. Maçanita, M. J. Calhorda, A. Charas, J. Morgado, M. T. Duarte, *Dalton Trans.* **2013**, *42*, 16969.

[18] M. J. Calhorda, D. Suresh, P. T. Gomes, R. E. Di Paolo, A. L. Maçanita, *Dalton Trans.* **2012**, *41*, 13210–13217.

[19] C. S. B. Gomes, C. A. Figueira, P. S. Lopes, D. Suresh, P. T. Gomes, M. T. Duarte, *Acta Crystallogr. Sect. C* **2011**, *67*, o315–o318.

[20] T. Yasumoto, T. Yamagata, K. Mashima, *Organometallics* **2005**, *24*, 3375–3377.

[21] P. J. Figiel, A. Sibaouih, J. U. Ahmad, M. Nieger, M. T. Raeisaenen, M. Leskelae, T. Repo, *Adv. Synth. Catal.* **2009**, *351*, 2625–2632.

[22] A. Ali-Bey, H. F. Loukil, G. Gosselin, A. Mathieu, A. Mesli, *J. Heterocycl. Chem.* **1982**, *19*, 617–624.

[23] M. Asadi, M. H. Ghatee, S. Torabi, K. Mohammadi, F. Moosavi, *J. Chem. Sci.* **2010**, *122*, 539–548.

[24] B.-C. Xu, T. Hu, J.-Q. Wu, N.-H. Hu, Y.-S. Li, *Dalton Trans.* **2009**, 8854–8863.

[25] J. Pommerehne, H. Vestweber, W. Guss, R. F. Mahrt, H. Bässler, M. Porsh, J. Daub, *Adv. Mater.* **1995**, *7*, 551–554.

[26] a) C. Hansch, A. Leo, R. W. Taft, *Chem. Rev.* **1991**, *91*, 165–195; b) M. Segala, Y. Takahata, D. P. Chong, *J. Mol. Struct. THEOCHEM* **2006**, *758*, 61–69.

[27] See, for example: a) B. Foresman, M. Head-Gordon, J. A. Pople, M. J. Frisch, *J. Phys. Chem.* **1992**, *96*, 135–149; b) M. Head-Gordon, R. J. Rico, M. Oumi, T. J. Lee, *Chem. Phys. Lett.* **1994**, *219*, 21–29; c) M. Head-Gordon, D. Maurice, M. Oumi, *Chem. Phys. Lett.* **1995**, *246*, 114–121.

[28] R. G. Parr, W. Yang, *Density Functional Theory of Atoms and Molecules*, Oxford University Press, New York, **1989**.

[29] a) SCM, ADF2009, Theoretical Chemistry, Vrije Universiteit, Amsterdam, The Netherlands, http://www.scm.com; b) G. te Velde, F. M. Bickelhaupt, E. J. Baerends, C. F. Guerra, S. J. A. van Gisbergen, J. G. Snijders, T. Ziegler, *J. Comput. Chem.* **2001**, *22*, 931–967; c) C. F. Guerra, J. G. Snijders, G. te Velde, E. J. Baerends, *Theor. Chem. Acc.* **1998**, *99*, 391–403.

[30] a) S. J. A. van Gisbergen, J. A. Groeneveld, A. Rosa, J. G. Snijders, E. J. Baerends, *J. Phys. Chem. A* **1999**, *103*, 6835–6844; b) A. E. Rosa, J. Baerends, S. J. A. van Gisbergen, E. van Lenthe, J. A. Groeneveld, J. G. Snijders, *J. Am. Chem. Soc.* **1999**, *121*, 10356–10365; c) S. J. A. van Gisbergen, A. Rosa, G. Ricciardi, E. J. Baerends, *J. Chem. Phys.* **1999**, *111*, 2499–2507; d) S. J. A. van Gisbergen, J. G. Snijders, E. J. Baerends, *Comput. Phys. Commun.* **1999**, *118*, 119–138.

[31] S. Portmann, H. P. Lüthi, *Chimia* **2000**, *54*, 766–770.

[32] F. Wang, T. Ziegler, *J. Chem. Phys.* **2005**, *123*, 154102–154113.

[33] SMART software for the CCD detector system, Version 5.625, Bruker AXS Inc., Madison, WI, USA, **2001**.

[34] SAINT software for the CCD detector system, Version 7.03, Bruker AXS Inc., Madison, WI, USA, **2004**.

[35] G. M. Sheldrick, SADABS, Program for Empirical Absorption Correction, University of Göttingen, Göttingen, **1996**.

[36] M. C. Burla, R. Caliandro, M. Camalli, B. Carrozzini, G. L. Cascarano, L. De Caro, C. Giacovazzo, G. Polidori, R. Spagna, *J. Appl. Crystallogr.* **2005**, *38*, 381–388.

[37] G. M. Sheldrick, SHELXL-97, A Computer Program for Refinement of Crystal Structure, University of Göttingen, Göttingen, **1997**.

[38] L. J. Farrugia, *J. Appl. Crystallogr.* **1999**, *32*, 837–838.

[39] M. N. Burnett, C. K. Johnson, ORTEP-III: Oak Ridge Thermal Ellipsoid Plot Program for Crystal Structure Illustration, Oak Ridge National Laboratory Report ORNL-6895, **1996**.

[40] R. F. Rodrigues, P. F. da Silva, K. Shimizu, A. A. Freitas, S. A. Kovalenko, N. P. Ernsting, F. H. Quina, A. Maçanita, *Chem. Eur. J.* **2009**, *15*, 1397–1402.

[41] G. Striker, V. Subramaniam, C. A. M. Seidel, A. Volkmer, *J. Phys. Chem. B* **1999**, *103*, 8612–8617.

[42] a) L. Versluis, T. Ziegler, *J. Chem. Phys.* **1988**, *88*, 322–328; b) L. Fan, T. Ziegler, *J. Chem. Phys.* **1991**, *95*, 7401–7408.

[43] S. H. Vosko, L. Wilk, M. Nusair, *Can. J. Phys.* **1980**, *58*, 1200–1211.

[44] A. D. Becke, *J. Chem. Phys.* **1988**, *88*, 1053–1062.

[45] a) J. P. Perdew, *Phys. Rev. B* **1986**, *33*, 8822–8824; b) J. P. Perdew, *Phys. Rev. B* **1986**, *34*, 7406–7406.

[46] E. van Lenthe, A. Ehlers, E. J. Baerends, *J. Chem. Phys.* **1999**, *110*, 8943–8953.

[47] a) J. P. Perdew, K. Burke, M. Ernzerhof, *Phys. Rev. Lett.* **1996**, *77*, 3865–3868; b) J. P. Perdew, K. Burke, M. Ernzerhof, *Phys. Rev. Lett.* **1997**, *78*, 1396–1396.

[48] Gaussian 09, M. J. Frisch, G. W. Trucks, H. B. Schlegel, G. E. Scuseria, M. A. Robb, J. R. Cheeseman, G. Scalmani, V. Barone, B. Mennucci, G. A. Petersson, H. Nakatsuji, M. Caricato, X. Li, H. P. Hratchian, A. F. Izmaylov, J. Bloino, G. Zheng, J. L. Sonnenberg, M. Hada, M. Ehara, K. Toyota, R. Fukuda, J. Hasegawa, M. Ishida, T. Nakajima, Y. Honda, O. Kitao, H. Nakai, T. Vreven, J. A. Montgomery Jr., J. E. Peralta, F. Ogliaro, M. Bearpark, J. J. Heyd, E. Brothers, K. N. Kudin, V. N. Staroverov, R. Kobayashi, J. Normand, K. Raghavachari, A. Rendell, J. C. Burant, S. S. Iyengar, J. Tomasi, M. Cossi, N. Rega, J. M. Millam, M. Klene, J. E. Knox, J. B. Cross, V. Bakken, C. Adamo, J. Jaramillo, R. Gomperts, R. E. Stratmann, O. Yazyev, A. J. Austin, R. Cammi, C. Pomelli, J. W. Ochterski, R. L. Martin, K. Morokuma, V. G. Zakrzewski, G. A. Voth, P. Salvador, K. J. Dannenberg, S. Dapprich, A. D. Daniels, O. Farkas, J. B. Foresman, J. V. Ortiz, J. Cioslowski, D. J. Fox, Gaussian, Inc., Wallingford, CT, **2009**.

[49] a) R. Ditchfield, W. J. Hehre, J. A. Pople, *J. Chem. Phys.* **1971**, *54*, 724–728; b) W. J. Hehre, R. Ditchfield, J. A. Pople, *J. Chem. Phys.* **1972**, *56*, 2257–2261; c) P. C. Hariharan, J. A. Pople, *Mol. Phys.* **1974**, *27*, 209–214; d) M. S. Gordon, *Chem. Phys. Lett.* **1980**, *76*, 163–168; e) P. C. Hariharan, J. A. Pople, *Theor. Chim. Acta* **1973**, *28*, 213–222.

[50] http://www.chemcraftprog.com/index.html.

[51] J. Morgado, A. Charas, J. A. Fernandes, I. S. Gonçalves, L. D. Carlos, L. Alcácer, *J. Phys. D: Appl. Phys.* **2006**, *39*, 3582–3587.

Received: September 11, 2013

FULL PAPER

Fluorescence

D. Suresh, P. S. Lopes, B. Ferreira, C. A. Figueira, C. S. B. Gomes, P. T. Gomes, R. E. Di Paolo, A. L. Maçanita, M. T. Duarte, A. Charas, J. Morgado, M. J. Calhorda*

■■ – ■■

Tunable Fluorophores Based on 2-(*N*-Arylimino)pyrrolyl Chelates of Diphenylboron: Synthesis, Structure, Photophysical Characterization, and Application in OLEDs

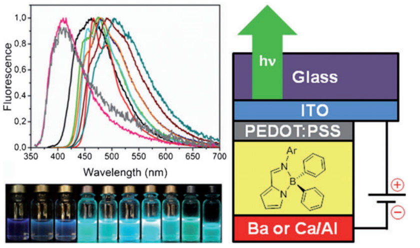

Fluorescent *N*,*N*′-boron chelate complexes: Mononuclear boron complexes of 2-(*N*-arylimino)pyrrolyl emit violet to bluish-green colors in solution (see figure, ITO = indium tin oxide, PEDOT:PSS = poly(3,4-ethylenedioxythiophene):poly(styrene sulfonic acid)), depending on the substituents on the *N*-aryl group. Organic light-emitting diodes have been successfully fabricated with the new boron complexes, achieving luminances of the order of 3000 cd m^{-2}.